Chemical Engineering Journal xxx (xxxx) xxxx

Contents lists available at ScienceDirect

Chemical Engineering Journal

journal homepage: www.elsevier.com/locate/cej

Review

Recent advances in 2D MXenes for enhanced cation intercalation in energy harvesting Applications: A review

N.R. Hemanth[a], Balasubramanian Kandasubramanian[b,*]

[a] Department of Metallurgical and Materials Engineering, National Institute of Technology Karnataka (NITK), Surathkal, India
[b] Nano Texturing Laboratory, Department of Metallurgical and Materials Engineering, Defence Institute of Advanced Technology (DU), Ministry of Defence, Girinagar, Pune, India

HIGHLIGHTS

- Discussion on 2D MXenes as novel material for lithium storage.
- Explores the mature synthetic routes to achieve high quality MXene layers.
- Parse the structure and miscellaneous properties.
- Deliberation on Lithium battery and Supercapacitor electrodes.
- Comparison between convectional electrodes and MXene electrodes.

GRAPHICAL ABSTRACT

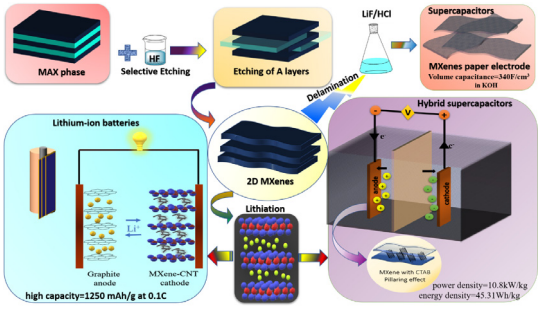

ARTICLE INFO

Keywords:
MXenes
Surface terminations
Selective etching
Energy storage

ABSTRACT

An advanced energy harvesting device that can be powerful with rapid storage mechanism, effective conservation, intact and secure recycling presently fascinate and are increasingly developed with the proper synthesis strategy and combination of nanomaterials with complementary properties. In 2011 extensive research has led to the wide emanating family of two-dimensional (2D) multi-layered transition metal carbides, carbonitrides and nitrides in conjunction with surface terminations namely fluorine, hydroxyl or oxygen which add hydrophilicity to their surfaces, these are collectively known as MXenes, they are derived from a selective etching of atomically thin sheets of 'A' element from MAX phases in the acidic solutions which contain aqueous fluoride. The gifted chemistry and unique morphology of MXenes allow us to use them for distinct applications which includes energy storage, electromagnetic interference shielding, anti-bacterial activity, nanofiltration of water, reinforcements, nuclear waste management, and catalysis. The excellent properties inclusive of high lithium (Li) storage capacity, rapid diffusion of Li, and low operating voltage make the MXenes a promising electrode, the macroporous $Ti_3C_2T_x$ sheets display gravimetric nearly 210 Fg^{-1} at scan rates of 10 Vs^{-1} which exceeds finest carbon supercapacitor and MXene hydrogels can have volumetric capacitances nearly 1500 $F{\cdot}cm^{-3}$. In this context, this review provides state of the art for the synthesis of MXenes, it's structure, intercalation, delamination, properties and thorough understanding between nanostructure and electrochemical performance which will encourage further study of 2D MXenes in energy harvesting applications.

* Corresponding author.
E-mail address: meetkbs@gmail.com (B. Kandasubramanian).

https://doi.org/10.1016/j.cej.2019.123678
Received 7 August 2019; Received in revised form 26 November 2019; Accepted 30 November 2019

1. Introduction

In the era of the 21st century, humans depend on wearable/portable electronic devices, and it is tough to picture a world without them as they have brought significant convenience and has dramatically altered lifestyles [1,2]. Considering ever increasing energy consumption requirements for these smart electronics and the exhaust of fossil fuels [3], viable energy alternatives inclusive of both large-dynamic energy storage and clean energy resources are crucially required [4]. Over recent years to ease the environmental hazard and energy storages, researcher's have been exploring renewable energy sources such as geothermal, hydroelectricity, tidal, and wind energy [4]. Simultaneously, energy from these renewable sources needs to be efficiently stored in electrochemical energy storage devices [4,5]. Lithium-ion batteries (LiB's) play a primary role in the current world, mainly in hybrid electric automobiles and portable wearable electronic gadgets [6]. The most constructive technologies of electrochemical energy storage are rechargeable lithium batteries and supercapacitors [7]. As leading energy conservation technologies, batteries and supercapacitor are a contrast to each other with respect of energy and power densities due to the dissimilar storage mechanism [4]. In short, batteries deliver elevated energy densities, but they endure from poor power densities that restrict their function in a field that requires more power [4]. At the same time, supercapacitors deliver excellent power densities, exceptional cycling stability, but suffer from low energy densities [4]. Researchers all over the world are exploring novel materials that can withstand exceptional energy and power density, that are also durable for a more extended period [8]. Presently most of the research activities have been devoted to 2D materials owing to their outstanding electrical, mechanical, optical properties, high aspect ratio, and they also feature an atomic level of thickness, these qualities make them remarkable in numerous applications. Many 2D materials can function as essential building blocks for a variety of layered structures, membrane, and composites [4]. Despite numerous single element 2D materials are synthesized, e.g., graphene, silicene, germanene, and phosphorene but the majority contains two or more elements, e.g., transition metal dichalcogenides (TMDs), layered double hydroxides [9]. Graphene has shown excellent research significance and has vast potential in energy storage and conversion applications [3,10].

In 2011, Gogotsi's group for the first time reported a new emerging constellation of graphene-like [11] 2D materials, early transition metal carbides, carbonitrides and nitrides which exhibited combination of metallic conductive nature and hydrophilic surfaces [12], and this family of 2D materials was termed as MXenes [6,13,14]. Their general formula is denoted by $M_{n+1}X_nT_x$ (n = 1–3) where M depicts transition metals (such as Sc, Ti, Zr, V, Nb, Hf, Ta, Mo and so on) [11], X stands for carbon and/or nitrogen, T_x is for surface terminations (such as hydroxyl, oxygen or fluorine) and x stands for number of surface terminations [9]. Some of the examples are $Ti_3C_2T_x$ and Ta_4C_3 [15], the n + 1 M layers of MXenes screen n X layers in $(MX)_nM$ pattern, the different structures of MXenes are shown in (Fig. 1) [9]. $Ti_3C_2T_x$ was the first MXenes synthesized, MXenes are typically synthesized by selective etching using hydrofluoric acid (HF) as etchant to remove the A layers from their corresponding MAX precursors, MAXs belong to family of layered ternary carbides or nitrides with general formula denoted by $M_{n+1}AX_n$ (n = 1–3) where M denotes early transitions metals as listed above, A is mainly group 13–16 elements and X is carbon and/or nitrogen, e.g., Ti_3AlC_2 [9]. Till date, over 60 different pure MAX precursors have been synthesized by researchers [16]. All the known MAX phases consist of a hexagonal layer with $P6_3/mmc$ symmetry [17], where M layers are almost closed packed, the X atoms fill the octahedral sites, and the A atoms are in turn attached with $M_{n+1}X_n$ layers [16]. In general, these laminated structures have an anisotropic property for the M−X bond, which possess strong mixed covalent or ionic or metallic behaviour, whereas M−A bond is purely metallic in nature [18]. The MAX bonds are too tough to be broken by application of shear or other mechanical means unlike other layered materials for example graphene and transition metal dichalcogenides where weak van der Waals forces hold the framework together [16]. The A atomic layers are chemically more functionalized, so the relative bond strength of interlayer M−A bonds and interatomic A-A bonds are weaker compared to M−X bonds, by taking advantage of difference in bond strength, chemical agents can be added to selectively etch out A layers without interrupting M−X bonds [4,16]. MXenes may contain one or more M element, and exists in two categories namely solid solution and ordered phases from the results of density functional theory (DFT) it is shown that the latter is energetically more stable than former one [9].

MXenes have a larger surface area, low diffusion barriers and superior electrical conductivity [19,20]; therefore, its application to electrode materials in LiB's and supercapacitors holds great promise [5]. The electrical conductivity of cold pressed, freestanding MXenes disks are almost comparable to multilayer graphene [6]. The carbon-based electrodes have shown volumetric capacitances up to 300 F per cubic centimetres, and hydrated ruthenium oxide has reached the capacitances up to 1000–1500 F per cubic centimetres [21]. MXenes (Ti_3C_2) has shown up to 300 F per cubic centimetres, additive free MXenes has high volumetric capacities of up to 1500 F per cubic centimetres [21,22]. The intercalation of lithium between the layers of graphite results in dilation up to 10% and suffer from severe structure collapse during high cycling rate [23], whereas sandwiched structure like $Ti_3C_2T_x$ has achieved outstanding cycling stability [24]. Ti_2AlC is most commercially and cheapest available MAX phase for the synthesis of MXenes [6]. Taking into account of all these factors functionalization of MXenes beyond graphene has been promising materials for electrode materials in LiB.

The synthesis of the very first MXene and extensive research has opened the door of large family of 2D materials for various practical application, although many challenging applications are yet to be focused and examined for future objectives [4]. In the present days, the following section has to be a central purpose to understand the complex nature of MXenes. Synthesis of unprecedented parent phases aside from MAX phases, alternative etching solutions rather than generally used HF, producing large scale high quality MXenes to study their atomic properties, examining the structure of MXene in much modern approach rather than DFT or molecular dynamics (MD) [9,16,25]. Controlling, tuning and achieving same kind of surface terminations in more facile way, understanding the intercalation of cations due to various surface termination and diffusion mechanism, study of heteroatomic doping to enhance the electrochemical performance, determining the change in magnetic, electric, optical and mechanical properties with respect to surface groups and additives, exploring various pragmatic application such as biosensors, arresting heavy metals and reinforcements, broadening the family by synthesis of new MXenes with modern approach and technology [15,16,18].

In this review, we select Ti_3C_2 as representative of MXenes and present its contemporary amelioration in energy harvesting applications and simultaneously, explore miscellaneous novel MXenes synthesized by modern methods which makes this review surplus capability, commensurate to other solitary literature. Beginning with the mere synthesis of $Ti_3C_2T_x$ via HF etching, followed by recent advancements to fabricate superior quality of unseasoned MXenes. The configurational structure, properties of bare MXene are discussed, and further reported on contingent of surface groups on the electrical and magnetic behaviour. Next the surface groups are concentrated, since conceptual and experimental results show that by eliminating surface terminations, lithium storage can be increased, but these surface groups are propitious in avoiding the restacking of 2D layered MXenes, which further facilitate in accelerated ion transfer. Besides lithium-ion and non-lithium-ion batteries and supercapacitors, devising of hybrid MXenes electrodes has been portrayed by exploiting carbon nanotubes (CNT) and cetyltrimethylammonium bromide (CTAB) which serves as a bridge gap between Ti_3C_2 interlayers and prevents restacking. These

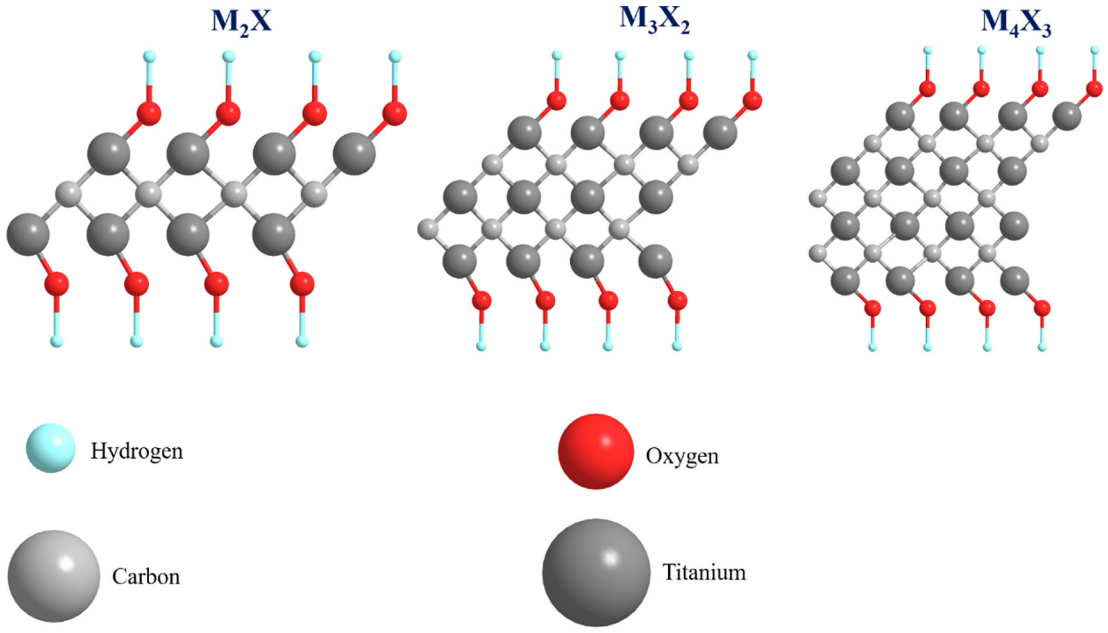

Fig. 1. Crystal structure of various layered MXenes with surface terminations as a hydroxyl group (−OH).

hybrid Ti_3C_2 electrodes provides enormous surface area and active sites for catalysis, thereby manifest sterling electrochemical performance compared to classical graphene electrodes. Finally, this review encourages the progression of $Ti_3C_2T_x$ cluster, fabrication of new-fangled MXene and augmentation of MXenes family for impressive electrode material for the future generation supercapacitor and batteries.

2. Modernistic techniques for synthesis of MXenes.

High-quality 2D MXenes are basically fabricated by selective etching of thin metal layers of A elements from their parent MAXs phases in the presence of chemical etchants like concentrated hydrofluoric acid (HF), ammonium hydrogen difluoride (NH_4HF_2) and ammonium fluoride, once the A layers are removed and they are substituted by surface groups (hydroxyl, fluorine and oxygen) so the correct representation of MXene is $M_{n+1}X_nT_x$ where T designates to surface terminations (Fig. 2a) [21,26]. Production of MXenes are categorized in two ways, top-down and bottom-up synthesis, the former approach is based on the etching of specific metallic layers using HF solution, while the latter process is considerable for producing ultrathin 2D MXenes by chemical vapor deposition with fewer faults and large lateral surface [4,27]. Naguib et al. described the synthesis of MXenes by dissolving MAX powder in an aqueous solution of HF of specific concentration followed by stirring, centrifugation, filtration and washing the precipitate with deionized water until pH value reaches between 4 and 6. As a result, accordion-like structures (Fig. 2b) are produced from solid MAX phase [28]. Among 10 different A elements, only aluminium (Al) has been successfully etched [28]. Chen et al. showed that the partial etching of $Ti_3C_2T_x$ resulted in higher capacitance (160 mAh/g) compared to fully etched (110 mAh/g) and 99% of capacity retention was observed after 1000 cycles [29]. Reactions steps that occur during etching of Ti_3AlC_2 with HF is given below [30,31].

$$Ti_3AlC_2 + {}_3HF \rightarrow AlF_3 + 3/2H_2 + Ti_3C_2 \quad (1)$$

$$Ti_3AlC_2 + {}_2H_2O \rightarrow Ti_3C_2(OH)_2 + H_2 \quad (2)$$

$$Ti_3AlC_2 + 2HF \rightarrow Ti_3C_2F_2 + H_2 \quad (3)$$

Various HF etching conditions for the synthesis of different MXenes and corresponding MAX phase with *c* lattice parameters are summarized in Table 1 [16]. Studies have shown that for many MXenes, there are no precursor ternary carbide MAX produced and synthesis of new layered MAX phases has to be researched [9]. For the first time Zhou et al. reported the synthesis of $Zr_3C_2T_x$ from the non-MAX phase, $Zr_3Al_3C_5$ which was prepared by pulse electronic sintering of zirconium (Zr), Al, and graphite powders. Nearly 1 g of $Zr_3Al_3C_5$ powder was added 10 ml of 50% HF at room temperature, after 72 h the left-out suspension was cleaned using deionized water and alcohol, later it was kept for drying for 48 h at room temperature to produce Zr_3C_2 [32]. In the recent studies it has been predicted that etching of Al-carbon units is more convenient than etching of Al layers from $Zr_3Al_3C_5$ [9], there are also reports on the etching of two A layers of Gallium from Mo_2Ga_2C to produce Mo_2CT_x [33] and etching of Al_3C_3 from $U_2Al_3C_4$ to form U_2CT_x [34]. Even though HF is widely used as etching agent, it is difficult to handle toxic HF in practical applications [4]. Xiong et al. introduced the modern approach of use of much milder and safer etchants by performing reaction between hydrochloric acid (HCl) and molten fluoride salts (LiF) which resulted in the removal of aluminium layers from Ti_3AlC_2 the synthesized material gets hydrated, swells and forms clay like shape (Fig. 2c), large $Ti_3C_2T_x$ flakes with fewer defects produced from in situ process has yield of almost 100% and the *c* lattice parameter was nearly 40 Å whereas $Ti_3C_2T_x$ flakes synthesized from HF has lattice parameter of 20 Å [4,21]. When high electrical conductivity and laterally large flakes are desired, LiF-HCl etchant is preferred, these deuterogenic process selectively etch A element simultaneously cations (Li^+, Na^+, K^+, Ca^+, Al^+, and NH_4^+) are intercalated between the layers of $Ti_3C_2T_x$ with exceptional features such as altered surface chemistry and enlarged interlayer spacing [4,5]. $Ti_3C_2T_x$ can also be obtained from their corresponding MAX phases by using FeF_3/HCl mixture, which reduces fluorine content and avoids the formation of secondary phase ($TiOF_2$) [35]. Although wet etching has been widely used for the synthesis of MXenes, the research on physical properties of MXenes have been hindered due to small layered flakes and low-quality crystals [27]. Gogotsi. discussed that the high-quality perfect crystals of molybdenum carbide (α-Mo_2C structure) are developed on bilayer substrate of copper foil upon molybdenum foil by chemical vapor deposition of methane (Fig. 2d) [9,27]. The crystals grown will have hexagonal, triangular shape and size exceeding 100 μm, these results make the facile study of intrinsic properties compared to solution formed flakes which have a lateral size less than 10 μm and the key for achieving ultrathin α-Mo_2C crystals is by maintaining a temperature

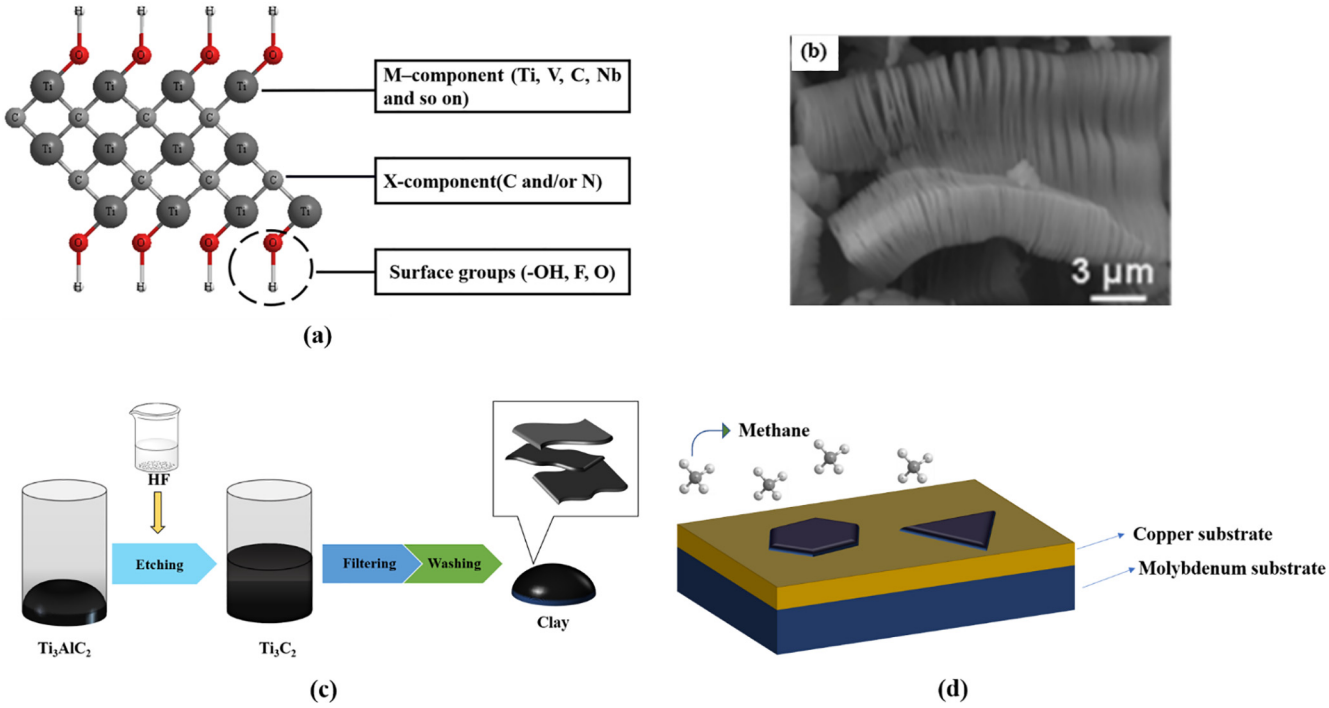

Fig. 2. (a) Side view of 2D MXenes synthesized from MAX phases. (b) Scanning electron microscopic image of HF etched Ti_3AlC_2 [16]. (c) In situ formation of HF produces swollen MXenes which resembles clay like shape. (d) Hexagonal or triangular shape ultrathin α-Mo2C formed by chemical vapor deposition in the presence of methane.

above 1085 °C, and low concentration of methane, also accelerated cooling after vapor deposition is crucial to obtain clean Mo_2C crystals [36]. The elimination of A elements from MAX phases can be prepared by heating the molten fluoride salts at high temperature in the gaseous atmosphere [37], Ng et al. reported that the synthesis of MXenes from their parent $M_{n+1}AX_n$ phases can be possible by etching at high elevated temperature, but a fractional loss of layers and structural transformation are unavoidable. If the synthesis is carried out at high-temperature chlorination, then etching of both M and A elements occurs and leads to the formation of carbide-derived carbons [18]. Recently, Fang *et al.* mentioned that Ti_4N_3 was synthesized in argon atmosphere at 550 °C by treating Ti_4AlN_3 with mixture of molten post fluoride salts which resulted in the formation of cubic phases of ordered non-stoichiometry carbides stable that were stable up to approximately 800 °C. Hence it is prudent that, preparation of MXenes at elevated temperature must be monitored precisely and ensure proper control over the temperature so that cubic structure is not formed [38]. However, it is observed that M components are only limited to Ti, V, Cr, Nb, Ta, Zr and Mo [18]. For example, TiC_x was developed by heating (900 °C) Ti_2AlC with molten LiF that resulted in rock salt structure but not 2D carbides because of the treatment conditions [9]. If a MAX precursors are completely converted to MXenes(especially thinner M_2X sheets), then there will be enlargement in *c* lattice parameter, due to which the X-ray diffraction (XRD) pattern of (000 *l*) peaks will not only broaden but also drift to lower angles (Fig. 3b) [5,16]. Comparing all the synthesis process, the HCl and LiF solution has been observed as an efficient way to produce new MXenes [39]. To date, many MXenes are theoretically predicted, and the following MXenes are synthesized $Ti_3C_2T_x$, Ti_2CT_x, Nb_2CT_x, V_2CT_x, $(Ti_{0.5}Nb_{0.5})_2CT_x$, $(V_{0.5}Cr_{0.5})_3C_2T_x$, Ti_3CNT_x, $Ta_4C_3T_x$, and $Nb_4C_3T_x$ [28].

These various methods and their results are useful in determining the necessary conditions to synthesize the desired MXene such as choice of parent MXene, etching concentration, type of etching solution, and altered surface groups. Different applications need a different route of synthesis, and for example, energy storage requires HF as etching agent whereas electronic applications need HCl/LiF as etching agent. More research has to be concentrated on the preparation of additive free nanosheet MXene with an environment-friendly and cost-effective method.

Table 1
Synthesis conditions and *c* lattice parameter of various MXenes from their MAX counterparts.

MAX structures	MAX phases	MXenes	Etching conditions at room temperature HF Conc.%	Time(hours)	*c* Lattice parameter	MAX MXenes
211	Ti_2AlC	Ti_2CT	10	10	13.6	15.04
	V_2AlC	V_2CT_x	50	8	13.13	23.96
				90	13.88	19.73
312	Nb_2AlC	Nb_2CT_x	50	90	13.79	22.34
	$(Ti_{0.5},Nb_{0.5})_2AlC$	$(Ti_{0.5},Nb_{0.5})_2CT_x$	50	28	18.42	14.88
	Ti_3AlC_2	$Ti_3C_2T_x$	50	2	18.62	20.51
			40	20	17.73	20.89
413	$(V_{0.5},Cr_{0.5})_3AlC_2$	$(V_{0.5},Cr_{0.5})_3C_2T_x$	50	69	18.41	24.26
	Ti_3AlCN	Ti_3CNT_x	30	18	24.08	22.28
	Ta_4AlC_3	$Ta_4C_3T_x$	50	72	30.34	30.34
	Nb_4AlC_3	$Nb_4C_3T_x$	50	90	30.47	30.47

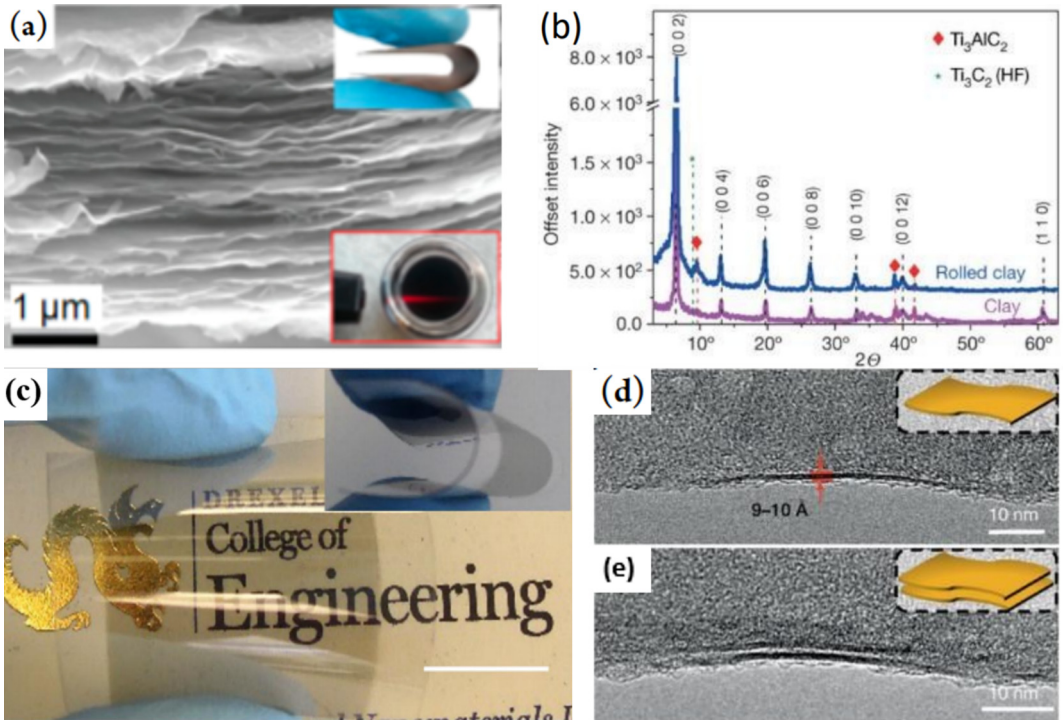

Fig. 3. (a) SEM image of $Ti_3C_2T_x$ paper prepared by filtering the additives from delaminated MXenes, the upper inset image is an optical image of $Ti_3C_2T_x$ paper bent between the finger without breaking, the lower inset is optical image of colloidal solution [28], (b) Measured XRD patterns of Ti_3AlC_2 and Ti_3C_2, before and after HF etching [18]. (c) Thin spray-coated $Ti_3C_2T_x$ film on a substrate shows high transparency, the inset image shows bending of $Ti_3C_2T_x$ films [9]. (d) Single layered $Ti_3C_2T_x$ and (e) Double layered $Ti_3C_2T_x$ [18].

3. Intercalation and delamination

In many 2D materials, intercalation is familiar phenomenon for which the strength of bonds between the layers is poor, this can be witnessed in materials such as clay and graphite [13,16]. The same applies for MXenes, which have weak bonds between the interlayers that facilitates in intercalation of several kinds of organic, inorganic, polymeric and ionic species (Fig. 8a, b, c1, c2) [16,40]. Intercalation of cations has gained a lot of attention owing to their unparalleled chemical and physical properties [13], as Xiong et al. reported that sliding of $Ti_3C_2T_x$ sheets was relatively easier when it was intercalated with cations such as Li^+ and it also modified the rheological properties [4]. Besides, Wang *et al.* demonstrated that Al ion intercalation led to horizontal sliding of Ti_3C_2X monolayer, appertaining to these results the structure of Ti_3C_2X monolayer was redefined [40]. Halim et al. explained that "gluing" of MXenes layers was observed because of strong interactions between layers when ammonia was intercalated between them using NH_4HF_2 and also mentioned that the resistivity of MXenes was increased when organic compound was introduced [41]. As intercalation chemistry is the key feature for energy storage, Li^+ ion charge storage mechanism in $Ti_3C_2T_x$ was analysed using in situ X-ray absorption spectroscopy (XAS), which revealed that during charging and discharging there was constant variation in oxidation state of transition metal up to 0.5 V versus Li/Li^+. Intriguingly, when potential was further reduced, there was no change in oxidation state. Instead lithium formed additional layer which bolstered the capacity by twofold and this mechanism was noticed in other MXenes [9]. Li et al. described that gravimetric capacitance of Ti_3C_2T can be enhanced by intercalating potassium ion (K^+) ion and surface terminals were modified, the resulting gravimetric capacity reached 517 F/g at a discharge rate of 1 A/g which was three times greater than pristine MXene [42]. Using MD derived XRD patterns, several N_2H_4 molecules that intercalated between the layers of $Ti_3C_2(OH)_2$ were compared and it displayed that molecules were arranged in the direction parallel to MXene basal plane and developed a monolayer [16]. Usually increase in the *c* lattice parameter is a consequence of intercalation, for example change in lattice parameter for Ti_3C_2X ranges from 0.7 Å for sodium sulphate and 15.4 Å for dimethlysulfoxide [16]. On intercalation of water, the *c* lattice parameter was significantly increased, which was due to hydration of these MXenes [43]. As Fredrickson et al. explained that Ti_2C and Mo_2C had one layer of oxygen under zero potential, irrespective of potential applied as bare MXenes were unstable and on application of voltage of ca. of −0.6 V, an adsorbate-mediated metal-insulator transition was revealed for Ti_2C, which established metallic Ti_2CH_2 system from insulating Ti_2CO_2 [43]. Ti_3C_2X delivered remarkable super capacitance when organic electrolyte was intercalated instead of commonly preferred solvents, this significant performance owes to stable wider electrochemical window of organic electrolyte and multi-valent cations [4]. As there was improved electrochemical performance due to intercalation of cation, further attempts were made to incorporate larger ions between the interlayers, as Chaudhari et al. mentioned that, it was practicable to intercalate large polyatomic cations like alkylammonium (AA) [44]. Using first principle simulation, Yu et al. investigated that, intercalation of Magnesium ion (Mg^+) in Ti_2C building block to form stable Ti_2MgC layered compound was favourable, the outstanding theoretical capacity, weak average cell potential and reasonable diffusion barrier of Mg^+ indicate that Ti_2MgC can be promising anode material [45]. The reduction in the first cycle irreversibility was only observed in Li^+ and Na^+ cation intercalation, good insight on multivalent and large ion incorporation would orient on progressive research and development of electrode materials [46].

To explore the properties that exist at the atomic level, delamination of $Ti_3C_2T_x$ is a necessary step [4,9,24] and higher rate capability is achieved by complete delamination of MXenes [47]. The simple delamination process is carried out by mechanical tape exfoliation where MXenes of thickness 10 μm are reduced to nanometres (Fig. 3d, e) [31] but the yield from this process was low [9]. Malaki et al. produced high-quality 2D sheets by ultrasonication as a principle tool for delaminating

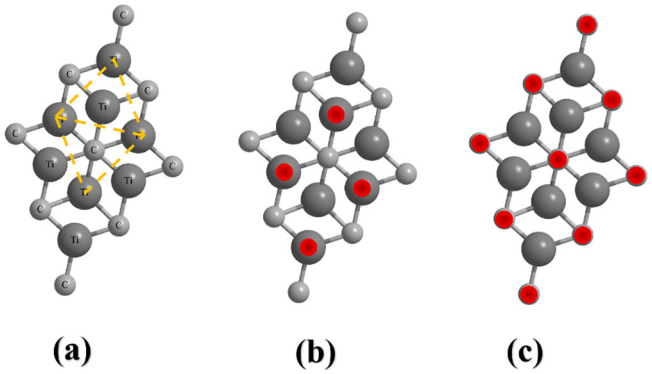

Fig. 4. (a) the top view of Ti3C2 layer, rhombus lattice (highlighted by dotted lines) with coordination number 6. (b) top view of configuration I. and (c) top view of configuration II, (red circles represent surface terminations). (For interpretation of the references to colour in this figure legend, the reader is referred to the web version of this article.)

and exfoliation [48]. High yield of delaminated MXenes was obtained by intercalation [16] of polar organic molecules [9] such as urea, formamide, and its derivative, dimethyl sulphoxide (C_2H_6OS), and long chain alkylamines [13]. Naguib et al. showed that multi-layers of MXenes when treated with tetrabutylammonium hydroxide (TBAOH) and then followed by sonication or agitation resulted in delamination, this approach was universal for several MXenes and has the potential for larger yield [17]. When HCl and LiF solution is used for etching, no external etchant is required since metal cations get intercalate, Further delamination takes by increasing the pH to neutral and then followed by mild hand vibration, resulted in stable suspension [9]. The delaminated $Ti_3C_2T_x$ after treating with HF formed transparent sheets of monolayers [4] as shown in (Fig. 3a, b).

4. Structure and properties

Modelling and fundamental understanding of properties, structure and surface interaction is a prerequisite in manipulating MXenes for diverse applications [16,18] the structure of first MXenes was predicted by density functional theory (DFT) [49]. A single layer of MXene has six-fold symmetry, hexagonal lattice and has coordination number of 6 (Fig. 4a), in the top view it has rhombus lattice (shown by dotted lines) (Fig. 4a) and in the side view, a single X layer is sandwiched between two M layers (Fig. 2a) [50]. The ordering of M in M_2X is ABABAB type (hexagonal closed pack), whereas the order of M in M_3X_2 and M_4C_3 are ABCABC type (face-centered cube), atomic ordering becomes a significant factor for the synthesis of transition metals such as molybdenum and chromium because it defines the stability of MXene with hexagonal closed packing [9]. For example, Mo_2CT_x is stable, but $Mo_3C_2T_x$ and $Mo_4C_3T_x$ are unstable because they follow ABCABC ordering and are stabilized by introducing Titanium in between the layers to form $Mo_2TiC_2T_x$ and $Mo_2Ti_2C_3T_x$ to form double-layered transition metal carbides [9,46]. Along with bare $M_{n+1}X_n$ layers, the properties of MXenes which are incorporated with surface terminations are predicted in recent studies [51]. Using transition electron microscope. Wang et al. reported that the surface groups are randomly distributed over the MXenes rather than a domain of specific kind of a group, the −F and −OH are directly bonded to superficies of MXene flakes [52]. On the basis of neutron scattering measurements, hydrogen bonding interaction occurs between −OH of one layer of $T_{i3}C_2T_x$ and −O, −F of another layer and van Der Waals force of attraction exists between the layers, the magnitude of hydrogen bond not merely depends on the orientation of −OH, but also relative scattering of hydroxyl groups on one surface to oxygen and fluorine groups on the other surface [52]. The surface terminations ratio depends on the etching concentrations, for example, 10% HF and HCl-LiF will have more oxygen and minimum concentration of fluorine compared to 50% HF [4,9,53]. From DFT studies [54] the orientation of surface terminations (T_x) are energetically favourable in two configurations, in configuration I (Fig. 4b) the T_x groups are situated on top of hollow space surrounded by three carbon atoms, in configuration II (Fig. 4c) the T_x groups are precisely on top of carbon atoms [16]. There is also mixed configuration III in which configuration I and configuration II lie on the opposite sides of MXene sheets, the relative structural stabilities of various $Ti_3C_2F_2$ and $Ti_3C_2(OH)_2$ configurations are as follows I > III > II, low stability was observed in configuration III because of steric hindrance between T_x groups and carbon atoms therefore fluorine (-F) and hydroxyl (−OH) functionalized MXenes tends to achieve configuration I [16]. The study of $Ti_3C_2T_x$ under X-ray photoelectron spectroscopy (XPS) divulges that it readily oxidises when exposed to air [9] as, Xie *et al.* discussed that oxygen (=O) and hydroxyl (−OH) terminated MXenes are more stable than fluorine (−F) terminated because, =O and −OH replace fluorine when stored and/or washed in H_2O atmosphere, further hydroxyl group are converted to oxygen when heated at high temperatures and/or during metal adsorption process [55]. Halim et al. discussed that the tuning of surface terminations can be achieved post-synthesis to meet the requirements of different applications [56].

Bare MXenes such as $Ti_{n+1}C_n$ have metallic character, concerning X atoms titanium nitrides evince better metallic character than titanium carbides since nitrogen possess one extra electron than carbon [15]. Notwithstanding, as the number of *n* increases, the metallic behaviour decreases simply because of additional Ti-X bonds [15]. The analysis of DFT and MD anticipate that among 2D MXenes, M_2C are more stronger and stiffer compared to M_3X_2 and M_4X_3 counterparts (Fig. 5a) [9,57,58]. MXenes whose surface terminations are functionalized by oxygen exhibit high mechanical strength and small lattice parameter compared to fluorine and hydroxyl groups, W_2CO_2 displays highest mechanical strength along with c11 which is equivalent to 592.7 GPa [59]. Recently Lipatov et al. performed nanoindentation using atomic force microscope for a monolayer of $Ti_3C_2T_x$ and reported highest Young's modulus value of 0.33 ± 0.03 TPa, which is highest compared to all solution prepared 2D materials [60]. A large number of MXene-polymer composites are prepared, for example, ultrahigh molecular weight polyethylene and Ti_3C_2 are blended, which enhanced tensile, breaking strength and also creep performances [61,62]. Thin MXene films (< 20 nm) intercalated epitaxially etched using NH_4HF_2 solution transmit 90% of the light from visible to the infrared region [41]. Recently Hantanasirisakul *et al.* proposed a elementary method to synthesize homogenous transparent $Ti_3C_2T_x$ films by spray coating delaminated colloidal $Ti_3C_2T_x$ solution over various substrates, ultraviolet–visible (UV–vis) spectrophotometry results for 5 nm thick films revealed transmittance of 91.2% and comparatively thicker film of 70 nm revealed 43.8% transmittance (Fig. 5c) [63]. There was a trade-off between conductivity, transmittance for thickness of films, instinctively a trade-off between transparency and conductivity depends on the thickness of MXene films [63]. Ali et al. fabricated transparent and thin $Ti_3C_2T_x$ films by electrohydrodynamic atomization process in vacuum free surrounding under the influence of the electric field at optimum temperature on a glass substrate, a thin 135 nm film exhibited low resistivity of $3.4 \times 10^{-4}\ \Omega-cm$, ~86.7% transmittance with superior diode behaviour of 120 mA at 3 V was recorded [64]. From the results of hybrid DFT calculations, Si et al. detailed that the ferromagnetism in Cr_2C due to d shell electron which are completely spin-polarized near to Fermi surface area, upon addition of surface terminations Cr_2C undergoes metal-insulator transition along with ferromagnetic to antimagnetic transition [65]. Kumar et al. predicted the magnetic properties of MXenes by developing crystal field theory-based model, the results showed that Mn_2NT_x behaved as highly ferromagnetic material at ground state, although magnetic nature vanishes in the presence of surface groups [66].

The examination of various MXenes have shown that the electronic properties vary from metallic to semiconductor, based on M, X and

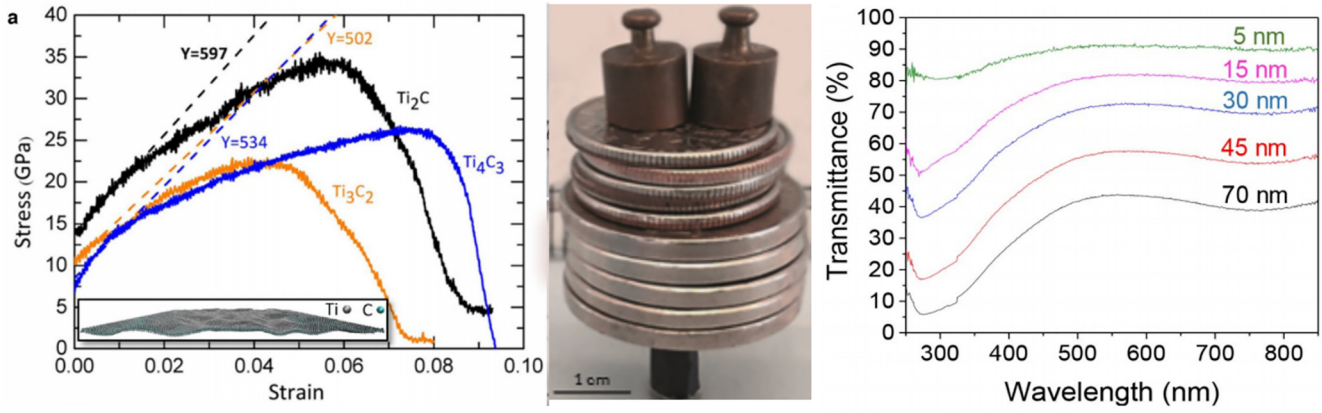

Fig. 5. (a) The stress–strain curves obtained from tensile test results of $T_{n+1}C_n$ samples using molecular dynamics [9]. (b) A hollow cylinder made from a thin 3.9-μm strip of 90 wt% $Ti_3C_2T_x$–poly vinyl alcohol composite, can withstand a load of 15,000 times of its own weight. The loads used are nickels (5 g), dimes (2.27 g) and weight of 2.0 g [9]. (c) Ultraviolet spectra of $Ti_3C_2T_x$ of different thickness produced by spray-coating [9].

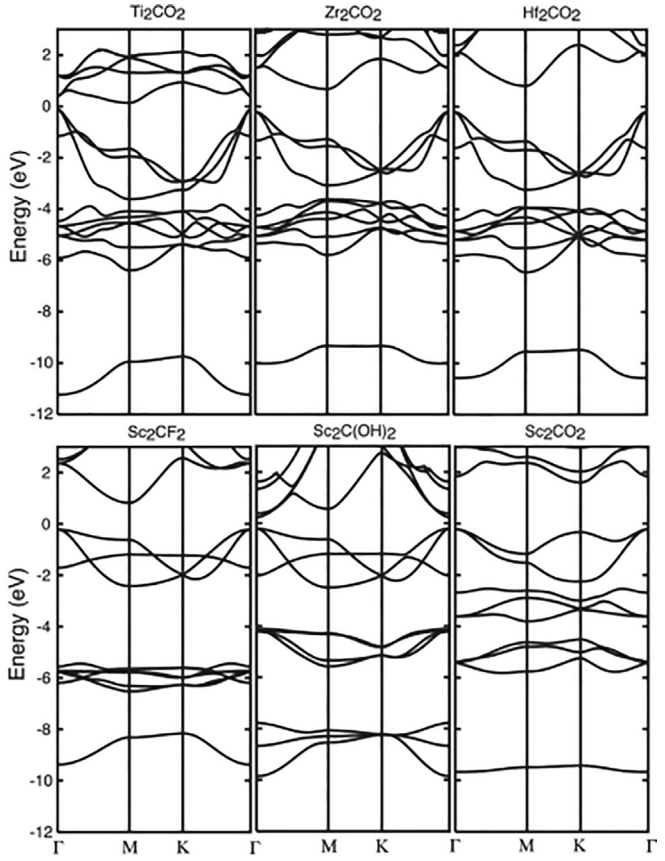

Fig. 6. The band gap of various MXenes, when the Fermi level is zero [51].

surface groups, the monolayers of MXenes exhibit metallic character with high electron density near Fermi level [67,68]. From band structure calculations, Khazei *et al.* obtained the energy gaps for Sc_2T_2(T = F, OH, and O) as 1.03, 0.45 and 1.8 eV and for Ti_2CO_2, Zr_2CO_2, Hf_2CO the energy gap was 0.24, 0.88, and 1.0 eV (Fig. 6a), the metallic to semiconducting behavior of Ti, Zr and Hf MXenes system near Fermi energy are similar because they belong the same group in periodic table, in addition, the effect on electronic character due to −OH and −F groups are the same since both surface termination can accept one electron from the surface [51]. Kim et al. obtained the values of work function for $Ti_3C_2T_x$ system (Table2), the significant variation in work function is mostly attributed to different surface groups, and measurement technique and highest electrical conductivity was observed as 10^4 Scm^{-1} for $Ti_3C_2T_x$ MXenes [69]. The electronic behavior of MXenes also depends on their thickness *'n'* [70], Xie and Kent. demonstrated that Ti_2CO_2 exhibit semiconducting behavior due to orbital hybridization of Ti 3*d* and O 2*p* close to Fermi level, for thicker MXenes ($n > 5$) the density of state vicinity to Fermi level was 3.5–8 times higher than thinner MXenes [67]. The research on surface variation of the MXenes, use of other components along with MXenes to prepare composites remain at most interest [18].

5. Applications

5.1. Lithium-ion batteries (LiBs)

Portable consumer electronic devices as a ubiquitous front runner and are integrated with rechargeable battery units are still limited to their application, MXenes have shown excellent electrical conductivity, low diffusion barriers (0.05 and 2.5 V versus Li^+/Li) [71], low operating voltages with high performance and large intercalation has made promising anode electrode material for LiBs [18,72]. The diffusion of cation between MXene layers takes at a higher rate as Levi et al. described that the presence of water between the swollen sheets of MXenes facilitated the rapid interaction of cations [73]. The larger specific area provides vast space for cation intercalation, Ren *et al.* reported that porous-$Ti_3C_2T_x$/CNT composites electrodes has shown the great capacity of 1250 mAh/g at 0.1C, which was relatively higher than

Table 2
The work function of $Ti_3C_2T_x$ MXenes system obtained by various methods.

Methods for calculating work function	Obtained work function (eV)
Ultraviolet photoelectron spectroscopy (UPS) under vacuum	4.37
Photoelectron spectroscopy in the air (PESA)	4.60
Kelvin Prove atomic force microscope (KPFM) under specific atmosphere	5.28

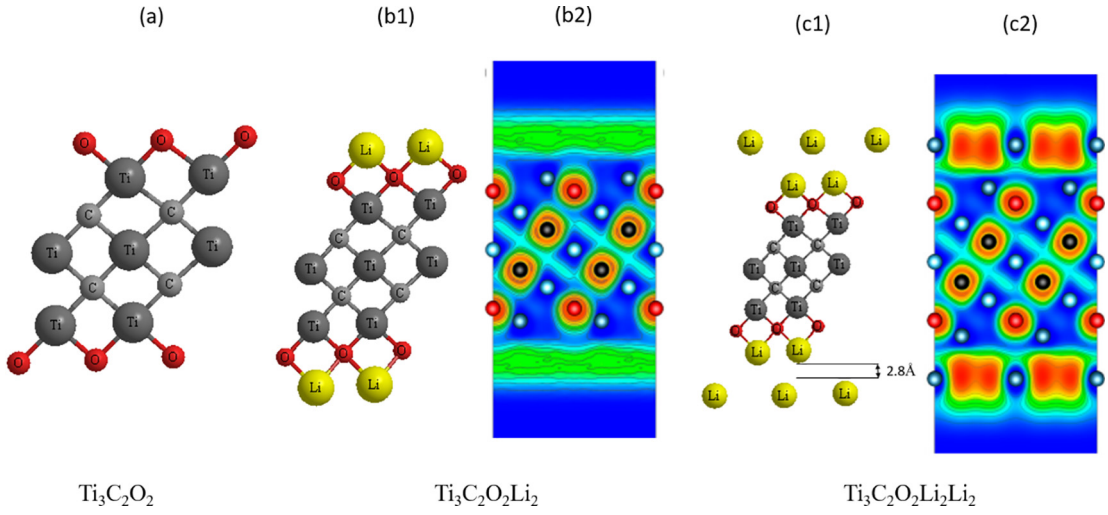

Fig. 7. (a) layered structure of Ti_3C_2 with oxygen as surface group. (b1) and (b2) lithiation on $Ti_3C_2O_2$ MXenes [55]. (c1) and (c2) extra layer of lithium on the surface $Ti_3C_2O_2Li_2$ [55].

non-porous $Ti_3C_2T_x$/CNT [26].Theoretical gravimetric capacitance and formation of stable interaction can be determined for simple lithium interaction reaction from the following mathematical equations, the current rate is assumed to be 1C [47].

$$M_2CT_x + 2Li \rightarrow M_2CT_xLi_2 \quad (4)$$

$$Q = \frac{nF}{m_f} \quad (5)$$

$$V = \frac{-[E(M_2CT_xLi_2) - E(M_2CT_x) - 2\mu(Li)]}{2} \quad (6)$$

where n stands for number of e^- passed per formula unit (in case of Li^+, K^+ and Na^+ the n value is 2, for Mg^{2+} it is 4), F is Faraday constant, M_f is total mass of formula unit, $E(M_2CT_x)$ stands for total energy of MXene before intercalation, $E(M_2CT_xLi_2)$ refers to energy of MXene after two cations are intercalated per formula unit and μ(Li) stands for chemical potential of intercalated cations [47]. If the value of Eq. (3) is positive then it suggests that the intercalation processes is favourable [47].

Zhang et al. produced high ordered transparent, large flakes of $Ti_3C_2T_x$ by spin casting followed by 200° annealing which resulted in an efficient material for charge storage with areal (0.48 mF cm^{-2}) and volumetric capacities (676 Fcm^{-3}), the asymmetric devices demonstrated gradual increase in capacities for over 20 000 cycles with 100% columbic efficiency [74]. Although moderate gravimetric capacity was observed, Kim et al. described that additive free cold pressed (1 GPa pressure) Ti_3C_2 films produced ~300 mm thick free-standing disc, upon using them as anode electrode in lithium batteries exhibited initial reversible capacity of ~15 mAh/$cm^{2,}$ and then it decreased up to ~5.9 mAh/cm^2 at C/3 after 50 cycles exceeding the performance of carbon-based electrodes [75]. Fu et al. flexible free-standing paper electrode of $Ti_3C_2T_x$, which exhibited ultrahigh volumetric capacitance of 892 F/cm^3 with high cyclic efficiency up to 10,000 cycles, these results were comparable to $Ti_3C_2T_x$ clay [76]. From the analysis of DFT, Zhang *et al.* described that by lowering the diffusion energy, increasing the lithium adsorption energy and after prudent tailoring of surface terminations, the $Ti_3C_2T_x$ films have shown satisfying reversible capacitance of 200 mAh/g at current density of 0.1 C for lithium-ion batteries [19]. To increase the electrical conductivity by impending aggregation and improving electron mobility, Zou et al. directly reduced $AgNO_3$ and fabricated Ti_3C_2/Ag composite electrode in the MXene atmosphere, this new electrode exhibited excellent reversible capacity of 310 mAh/g at 1C after 800 cycles, 260 mAh/g at 10 C after 1000 cycles and 150 mAh/g at 50 C after 5000cycles, the long life cycle is observed due to decrease in interference resistance and formation of Ti (II) and Ti (III) [77].

It was observed that the existence of surface terminations on the bare MXenes has drastically reduced its capacities [9]. From DFT analysis, Tang et al. reported that the bare monolayers of Ti_3C_2 (320 mAh/g) has higher lithium capacitance and drastically reduced upon addition of surface groups like hydroxyl or fluorine, fully terminated hydroxyl and fluorine MXenes have shown lithium storage capacities of 67 mAh/g and 137 mAh/g respectively [11]. The cation capacity of MXenes is not fully defined by formula weight as, Naguib *et al.* reported V_2CT_x MXene showed highest lithium ion capacity (280 mAh/g at 1C and 12 mAh/g at 10 C) compared to $Ti_3C_2T_x$ MXene (110 mAh/g at 1 C) although niobium is more heavier than titanium the gravimetric capacity was found to be higher in $Nb_2C_2T_x$ (180 mAh g^{-1} at 1 C) this was explained by complex nature of surface termination [78]. As discussed earlier about oxygen-terminated surface groups, Eames *et al.* predicted that oxygen terminated MXenes are found to have higher capacitance compared to hydroxyl and fluorine groups[47] as, Xie et al. investigated surface terminations of lithiated $Ti_3C_2O_2$ and observed an extra layer of Li which enhanced the capacity (410 mAh g^{-1}) by facilitating the interactions between MXene layer and accessible volume for additional lithium layers (Fig. 7a–c) [55].

The addition of other nanoparticles such as carbon nanotubes acts as spacers and provide abundant space for intercalation of cations [14,23]. Multi stacked layers of MXenes exhibit lower capacities and reduced rate, Lin et al. described novel method to prepare $Ti_3C_2T_x$/CNF hybrid electrode for lithium battery by chemical vapor deposition, a superior reversible capacities of 320 mAh/g at 1C was observed by $Ti_3C_2T_x$/CNF materials and there was no decay up to 2900 cycles at 100C [79]. Boota et al. described the simple method to synthesize in situ polypyrrole/ Ti_3C_2 composite electrode have reported volumetric capacitances of ~1000F/cm^3 and efficient capacitive retentivity of 92% after 25,000 cycles, this attribution to increase in interlayer distances between $Ti_3C_2T_x$ sheets (Fig. 8a) [80]. To overcome moderate capacities, Luo *et al.* produced PVP-Sn (IV)@ Ti_3C_2 nanocomposites by polyvinylpyrrolidone (PVP)-assisted liquid-phase immersion method and observed high volumetric capacitance of 635 mAh/g at 100 mA/g, this was simply because of "pillar effect" of Sn between the interlayers and also the synergistic effect among alk-Ti_3C_2 matrix and the charge–discharge curves observed were similar to that of supercapacitors (Fig. 8b) [81]. *In-situ* XRD was employed to study energy storage mechanism, Dall 'Agnese *et al.* reported and compared electrochemical performance of Ti_3C_2 clay, fully delaminated and carbon nanotube composite of Ti_3C_2 electrode with organic electrolytes, the observed

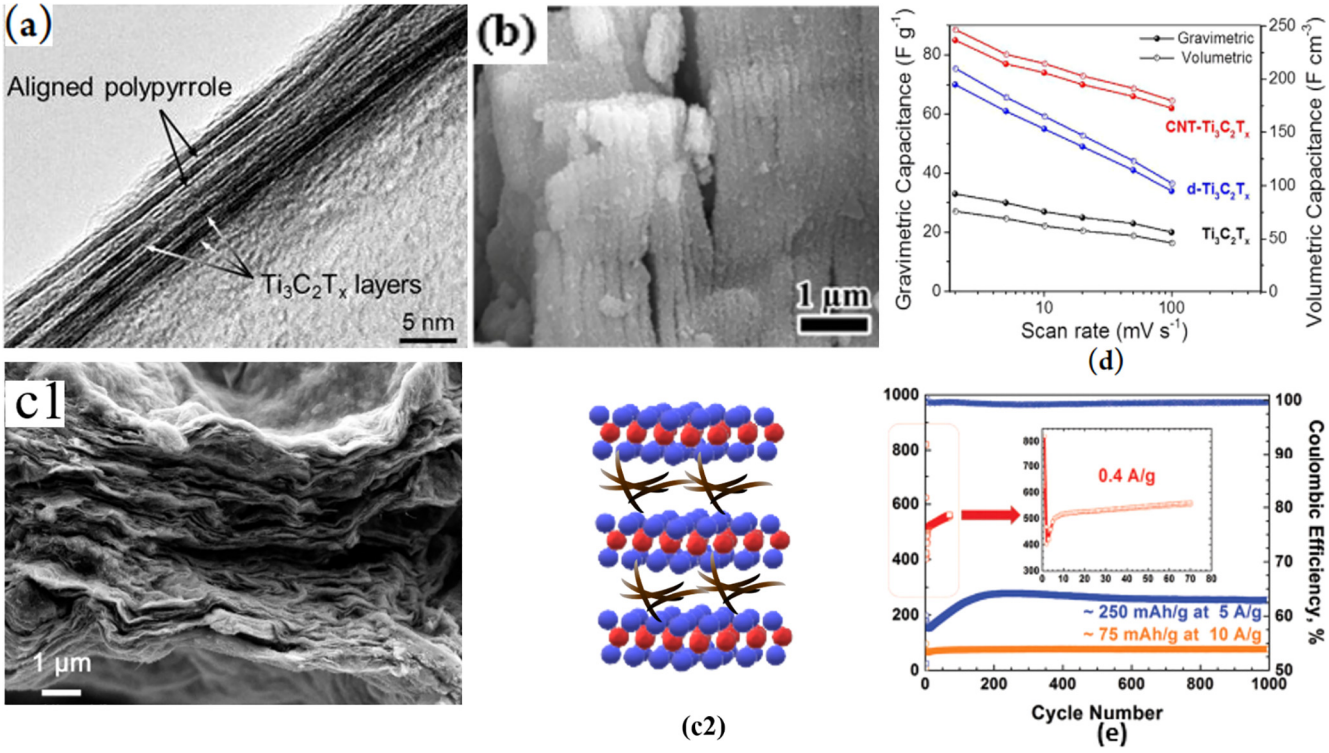

Fig. 8. (a) TEM images of cross section of polypyrrole (bright layers) between $Ti_3C_2T_x$ layers (dark layers) [80].(b) SEM images of PVP-Sn (IV)@ Ti_3C_2 nanocomposites with Sn between the layers [81]. (c1) SEM images of CNT- $Ti_3C_2T_x$ nanocomposites [82]. (c2) CNT between the $Ti_3C_2T_x$ layers. (d) The gravimetric capacitance for various scan rates and corresponding scan rates [82]. (e) Summary of capacitance and number of cycles at different rates and corresponding efficiency [33].

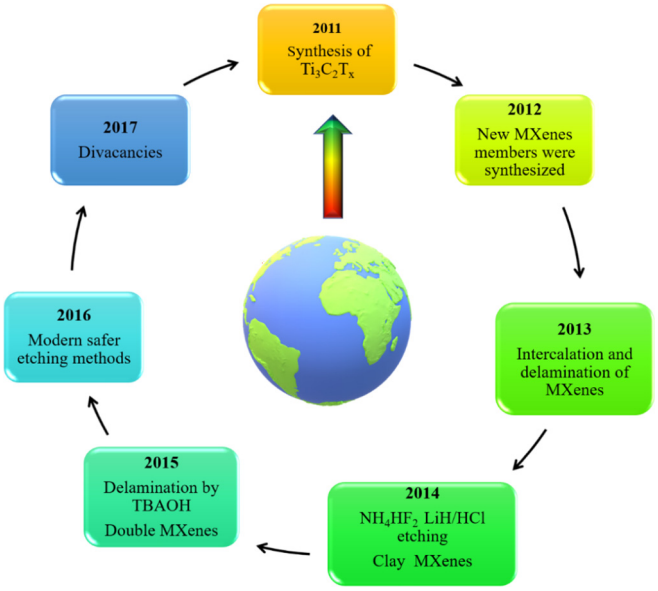

Fig. 9. Timeline of MXenes and recent their advances over last decades [24].

capacitance was 32 F/g and 85 F/g for clay MXene and delaminated MXenes respectively and capacitance of 254 F/m at 2 mV/s was shown by carbon nanotube/Ti_3C_2 composite electrodes which provided increased accessibility of the cations (Fig. 8c, d) [82]. Ti_2C has the highest surface area among all the potential MXenes and revels high gravimetric capacitance [71] later, Naguib *et al.* discussed that the gravimetric capacitance of Ti_2C was found to be at least 50% more than that of Ti_3C_2 MXenes and has exhibited high capacities at various scanning rates, this advancement in the change of capacity was observed because of one inactive layer of TiC in Ti_3C_2 [6]. Niobium-based electrodes are also widely studied after Ti_3C_2 electrodes, Mashtalir et al. explored the capacitance of delaminated Nb_2CT_x flakes by intercalation of propylamine, mild sonication and followed by vacuum filtering in CNT solution, this Nb_2CT_x/CNT electrode exhibited unprecedented volumetric capacities of 325F/cm^3 and 400 mAh/g at 0.5 C [83]. Byeon et al. tested three hybrid Nb_2CT_x/CNT electrodes that can be paired either as a battery anode type or battery cathode type as well as symmetric setup [84]. Although Nb_2CT_x exhibits high reversible capacity, they resemble more like an electrochemical character than lithium batteries [18]. Molybdenum-based electrodes are also explored, Halim *et al.* investigated Mo_2CT_x–CNT paper electrode of 3 µm thickness and tested it against lithium, high volumetric capacitance of 560 mAh/g at 0.4 A/g was observed along with 2/3 of lithium was stored under 0.5 V versus Li/Li^+ and found to be stable for over 1000 cycles (Fig. 8e) [33].

5.2. Supercapacitors

The energy storage mechanism of a supercapacitor is intermediate between battery and capacitor, it offers high power and energy densities [1,4,85], the performance of $Ti_3C_2T_x$ depends on various factors such as scan rate, cell configuration, and type of electrolyte. Supercapacitors are categorized into two main groups; the first category is electric double layer capacitor (EDLC) and the second one is pseudo capacitors which are more preferred because of high volumetric capacity due to Faradic reactions [4,20]. Paper $Ti_3C_2T_x$ capacitors have shown less resistance than multilayer $Ti_3C_2T_x$ as, Lukatskaya *et al.* described that few layers of $Ti_3C_2T_x$ paper electrodes nearly doubled the gravimetric capacitance and volumetric capacitance recorded in KOH solution was 340 F/cm^3 which was much higher than activated graphene (60–100 Fcm^{-3}), and carbon derived electrodes (180 Fcm^{-3}) [5]. In perspective for further improvement of $Ti_3C_2T_x$ electrodes, Ghidui *et al.* synthesized $Ti_3C_2T_x$ 'clay' by using LiF and HCl as etching agent, and recorded high volumetric capacity was 900 Fcm^{-3} and

gravimetric capacitance of 245 F/g, this improved capacities was observed due to high interlayering spacing formed by clay during the synthesis process [21]. Hu et al. fabricated $Ti_3C_2T_x$ films via dropping-mild baking approach and then loaded these binder free $Ti_3C_2T_x$ films uniformly on nickel foam, which exhibited high ultrahigh gravimetric capacitances of 499 F/g with exceptional cyclability [86].

Macroporous $Ti_3C_2T_x$ electrodes are used to push capacitance up to theoretical values as, Lukatskaya *et al.* investigated the $Ti_3C_2T_x$ hydrogel films prepared by immersing vacuum filtered $Ti_3C_2T_x$ colloidal solution in acetone for 72 h, the resulting $Ti_3C_2T_x$ hydrogel demonstrated areal capacitance up to 4 Fcm^{-2} and excellent volumetric capacity up to 1500 Fcm^{-3} surpassing the state-of-the-art of supercapacitor electrode materials [22]. Recently flexible solid-state supercapacitors were explored by, Dubal et al. assembled an asymmetric cell of transparent $Ti_3C_2T_x$ films and single-walled carbon nanotubes as positive and negative electrodes respectively, as a result, the cell displayed notable capacitance of 1.6 mF cm^{-2} with no decay over 20 000 cycles [1]. Alternatively, Jun et al. explored $Ti_3C_2T_x$ – reduced graphene oxides (rGOs) for asymmetric micro-supercapacitors, they displayed significant power density of 0.2 W/cm^3 and spelended energy density of 8.6 mWh/cm^3 under voltage window of 1 V and the 97% of capacitance was retained after 10 000 cycles [85]. Xie et al. prepared BiOCl nanosheets incapacitated on $Ti_3C_2T_x$ nanocomposite flakes via chemical bath deposition which exhibited attractive volumetric capacitances of 396.5 F/cm^3 at 1 A/g and 228 F/cm^3 at 15 A/g, high energy density of 15.2 Wh/kg with power density of 567.4 W/kg, which was higher than previous mentioned symmetric electrode [87]. Flexible energy storage system has more attracted for their application in portable and wearable electronic devices, recently, Zhang et al. synthesized $Ti_3C_2T_x$/Carbon Cloth (CC) flexible electrode by facile method of dipping and fast freezing, the results indicated areal capacitance of 191 mF cm^{-2} in 1 M H_2SO_4, with exceptional capacity of 97% was retained after 8000 cycles at current density of 4 mA cm^{-2}, further areal capacitance can be increased up to 312 mF cm^{-2} by alkalization and annealing to obtain ak-$Ti_3C_2T_x$/CC electrode [88]. Hybrid supercapacitors has been geared as a modern type of energy storage as, Luo et al. described that CTAB-Sn(IV)@Ti_3C_2 prepared by facile liquid phase CTAB prepillaring and Sn^{4+} pillaring process, the interatomic space was increased by 177% i.e, 2.708 nm compared to initial spacing of 0.977 nm, when CTAB-Sn(IV)@Ti_3C_2 anode was coupled with AC cathode, it exhibited significant capacitance retention of 71.1% after 4000 cycles at the rate of 2 A/g with columbic efficiency nearly equal to 100% [89]. It was confirmed that superior power density of 495 W/kg with high energy density of 105.56 Wh/kg was achieved, also when the power density was increased to 10.8 kW/kg the lithium ion capacitor was still able to deliver 45.31 Wh/kg which was directly dependent on the weight of CTAB-Sn(IV)@Ti_3C_2 [89].

5.3. Non-lithium batteries and other fundamental applications

The extensive utilization of lithium resources has led researcher's to focus on rechargeable non-lithium batteries, MXenes owing to their proficient nature in storing various cations like sodium(Na^+), potassium(K^+), calcium(Ca^{2+}), magnesium(Mg^{2+}) and aluminium(Al^{3+}) [4,5,9,24,47], the adsorbing capacity of Ti_3C_2 for Na^+, K^+, Ca^{2+} has been theoretically predicted as 351.8, 191.8, 319.8 mAh g^{-1} respectively [24]. Multilayer MXenes are of great interest in the field of electrochemical energy, however they are curtailed because of their poor capacity along with torpid sodiation kinetics, to surmount this, Luo et al. introduced sodium ion (Na+) between the Ti3C2 sheets to form pillared sheets of Na-Ti3C2 with decreased Na+ diffusion barrier and increased active site concentration and exhibited considerably high reversible capacity of 175 mAh/g at 0.1 A/g with exceptional cycling stability over 2000 cycles at 2 A/g, when Na-Ti3C2 was coupled with AC cathode, the assembly demonstrated remarkable energy density of 80.2 Wh/kg with high power density of 6172 W/kg and protracted cycling stability performance accompanied with notable capacity retention of approximately 78.4% at 2 A/g even after 15000 cycles [90]. From electrochemical measurements, Xie et al. reported that experimental discharge capacities of multi-layered $Ti_3C_2T_x$ for Na^+ and K^+ ion batteries are 370, and 260 mAh/g, respectively, corresponding to, 2.79Na, 1.96 K per $Ti_3C_2T_x$, furthermore regardless the size of cations the similar capacities of 100 mAh/g is observed after 100 cycles [91]. Sodium storage batteries has been potential surrogate to lithium storage batteries as, Luo et al. reported that the intercalation of Sn^{2+} the layers of Ti_3C_2 not only serves as nucleation and growth of Na within the layers, but also endows in large interatomic space for uniform deposition of Na contributing to pillar effect [7]. Therefore, the CT-Sn(II) @Ti_3C_2 prepared by prepillaring of CTAB, followed by Sn^{2+} pillaring highly stable anodes could achieve high current densities up to 10 mA cm^{-2} and substantial areal capacities up to 5 mAh cm^{-2} over 500 cycles [7]. In the recent years sodium batteries have fascinatingly attracted owing to their excellent safety and stability as, Guo et al. discussed that $Ti_3C_2T_x$ nanosheets demonstrated excellent reversible capacity of ~175 mAh/g, upon increasing the current density to 200–5000 mA h/g the capacities varied from 156 to 63 mAh/g [92]. Later to improve the sodium capacitance, Zhao et al. described that 3-dimensional macroporous $Ti_3C_2T_x$ film exhibited a discharge capacitance of 390 mAh/g at 2.5 C and reversible capacitance of 210 mAh g^{-1} with Columbic efficiency of 53.8% which was much higher compared to multilayer $Ti_3C_2T_x$ and $Ti_3C_2T_x$/carbon nanotube hybrid films [93]. The sodium storage capacity was further improvised by intercalating the sulphur atoms between the interlayer of Ti3C2 after successfully pretreating it with CTAB, during the annealing process when the temperature is 450oC, the sulphur intercalated CT-S@Ti3C2-450 electrode evidence with sodium storage capacity of 550 mAh/g at 0.1 A/g and exceptional cycling stability of 5000 cycles at the rate of 10 A/g due to augmented pseudocapacitance, which was verified by theoretical and kinetic analysis. When CT-S@Ti3C2-450 anode was assembled with commercial AC cathode, improved energy density of 263.2Wh/kg under exalted power density of 8240 W/kg with prominent cyclic performance was recorded [94]. Recently XRD and XPS were used to examine the K^+ storage mechanism as, Naguib et al. developed titanium carbonitride as an anode electrode for K^+ batteries, the results have shown that initial capacity of 710 mAh/g dropped to 275 mAh/g at the rate of 20 mA/g [95].

The structural architecture of MXenes with surface terminations exhibit versatile nature for its use in diverse applications. Although a majority of the application is based on energy storage, other potential applications of MXenes outperform several 2D materials [9], for example, hydrogen evolution reaction (HER) electrolysis approach has the ability to generate hydrogen as green energy and also it can be developed in large scale [96,97] and it was first reported by Seh et al. that MXenes can be used for the application of HER [98]. From the analysis of DFT calculations, electrochemical analysis, and an array of characterization methods, Handoko et al. showed that the occurrence of fluorine groups was deleterious for (HER), the inimical effects of fluorine terminations was not only just limited to Titanium based MXenes, but also explained for Molybdenum based MXenes [99]. These outcomes can be effectively used for designing novel materials for HER, when minimum overpotential is preferred or for energy harvesting, when maximum voltage is required [99]. To reduce the radical effects of climate change, sustainable energy conversion and storage play a crucial role, especially by electrocatalytic and photocatalytic reduction of carbon dioxide to valuable fuels and chemicals [100–102]. W_2CO_2 and Ti_2CO has been identified as promising materials for electrocatalytic reduction of CO_2, because of low overpotential on the surface that can be accomplished due to more energetically propitious *HCOOH path compared to *CO route and does not depend much on n–C coordinated intermediates [100]. And most importantly, $Ti_3C_2T_x$ sheets are known for excellent electromagnetic interference shielding comparable to that of graphene [103,104]. Other applications of

Table 3
Applications of MXenes other than energy storage and the corresponding MXenes.

Applications	Material	Explanation	References
Electromagnetic interference shielding	$Ti_3C_2T_x$, $Ti_3C_2T_x$/calcium alginate	Excellent shielding performance in aerospace and smart electronic devices.	[103,116]
Antibacterial Activity	$Ti_3C_2T_x$	Bactericidal properties to counter Escherichia coli (E. coli) and Bacillus subtilis (B. subtilis)	[112,117]
Photo catalysis	$Ti_3C_2T_x$, Ti_2CO_2, $Ti_3C_2(OH/ONa)_2$, Ti_3C_2 and g-C_3N_4 nanocomposites.	Dehydrogenation of hydrogen storage materials, CO oxidation, oxygen reduction reaction, oxygen evolution reaction (OER), and hydrogen evolution reaction (HER).	[97,102,118]
Thermal decomposition	Ti_3C_2-Cu_2O nanocomposites.	Decomposition of Ammonium perchlorate (NH_4ClO_4 or AP), a widely used rocket propellent.	[119]
Biosensors	(3-Aminopropyl) triethoxysilane functionalized Ti_3C_2	Highly responsive for carcinoembryonic antigen detection.	[120]
Radionuclide imprisoning	Hydrated $Ti_3C_2T_x$,	Capture of environmental hazards heavy metals such as Uranium (VI)	[121]
Gas sensors	$Ti_3C_2T_x$	Detection of volatile organic gases present in small quantity, so as to cure the disease at an early stage	[122]
Water Desalination	$Ti_3C_2T_x$ (similar to aerogel)	High adsorbing capacitive deionization (CDI) of saline water	[123]
Photo thermal	Ti_3C_2	Synergistic therapy for combating cancer eradication	[124,125]
Structural composites	$Ti_3C_2T_x$. Polyurethane	Addition of MXenes results in significant increase in yield stress, tensile strength and hardness.	[114]
Electronics field	Ti_2CT_x	Exhibit excellent field effect mobilities and band gaps can be altered by altering surface groups.	[31]
Dye absorption	alk-$Ti_3C_2T_x$	Modified surface group MXenes enhances rapid adsorption of methylene blue	[126]
Water purification	$Ti_3C_2T_x$ – Fe_2O_3	substantial selectivity and absorption of phosphate	[127]
Lubrication	$Ti_3C_2T_x$	Acts as additive lubrication in base oil	[9]

MXenes has also been investigated such as catalysis [105,106], biosensors [107–109], photothermal therapy [110], gas sensors [111], antibacterial activity [112], water purification [9,113], reinforcement composites [114] and resistive random-access memories (RRAMs) [115] (Table 3).

6. Conclusions

In the past five years, there has been substantial evolution in development of 2D carbides, carbonitrides and nitrides as energy harvesting materials and demonstrated remarkable performance comparable to graphene. The versatile structure and notable properties have attracted MXenes into disparate applications in present-day, among them especially $Ti_3C_2T_x$ has drawn significant amount of involvement and is epitome of promising electrode, biocompatible and flexible film material.

In this review, on the basis of theoretical, computational and experimental studies we have contemplated $Ti_3C_2T_x$ as energy storage device like rechargeable lithium batteries and supercapacitors. In general HF solution based and fluoride salt-based etching are endorsed for synthesis of MXene, HF synthesized MXenes are smaller in size and has more faults, whereas fluoride-based etching produces MXenes of larger flake size and good mechanical strength properties. The mechanical stripping process to obtain multilayers of MXene is also possible by embedding polar organic molecules between MXenes sheets followed by mechanical oscillation or sonication. The yields are significantly higher and procedure is facile and readily extendable and the use of non-aqueous etchants could avoid the oxygen and hydroxyl groups. Although the most constructive and commonly practised routes to synthesize $Ti_3C_2T_x$ is by selective etching of Ti_3AlC_2 precursors with HF solution, it is always preferable to use LiH-HF etchant which is relatively milder with high yield. The selective etching processes adds oxygen, hydroxyl and fluorine terminations to the bare MXenes and other mature synthesis routes are etching from non-MAX precursors, for example $Zr_3Al_3C_5$ to obtain $Zr_3C_2T_x$ and also CVD synthesis process to achieve high quality ultra-thin orthorhombic 2D α-MoC and other emerging MXenes which have been evaluated in succinct. XRD results provide sufficient evidence to substantiate whether MAX is entirely transformed into MXene and it is essential to tune the properties of $Ti_3C_2T_x$ for miscellaneous applications.

In general, the crystal of MXenes is hexagonal close packed structure which is identical to their parent structure and has coordination number 6. They are usually labelled as $M_{n+1}X_n$, where *(n + 1)* layers of M are in alternatively interfaced to (*n*) layers of X, the surface class is highly dependent on the synthesis technique and are arbitrarily disseminated. The theoretically calculated value of *c* lattice parameter by XRD method was imprecise with XRD results for completely hydrated MXene, albeit the fact that the mixture of fluorine and hydroxyl group were present. By vacillating the synthesis process, surface groups, degree of delamination and exfoliation can be tuned in desired fashion. The surface groups play decisive role in determining the properties and stability of MXenes, typically surface groups reduce conductivity and eliminates magnetic nature, MXenes with oxygen terminated are reasonably more stable compared to fluorine or hydroxyl group, practical insight on concept of surface distribution is very complex to understand. In addition to high conductivity, $Ti_3C_2T_x$ illustrate high mechanical properties and outstanding optical properties making it pertinent to define as promising flexible thin films and act as flexible electrode material in supercapacitors, by taking worth of diverse properties of $Ti_3C_2T_x$ makes it appropriate candidate in assorted applications which has been addressed in terse.

Due to synergistic effect in prevention of conglomeration, enhancing electrochemical permanence, improved pseudo capacitance and promoting electron conductivity, MXene based electrodes have opened a new door to diversified energy storage system. The 2D morphology and interface characteristics of $Ti_3C_2T_x$ facilitate in intercalation of many multivalent cations in between the layers, Li intercalation has been major attraction in recent years for their application in rechargeable LiBs. Apart from Li ions, MXenes are potential host for a variety of other cations including Na^+, K^+, $NH^{4\ +}$, Mg^{2+} and Al^{3+}, that can be intercalated electrochemically, while reaching exceptional capacities of over 300 F and anodized Ti_3SiC_2 used as Li ion micro batteries performed at various multiple current densities with an exceedingly areal capacity. MXene premised composite electrodes with metal oxides as filler material are imperative, because of immanent capacities, ancillary electrolyte ion access and conductive pathways has been achieved by incorporation of spacers like transition metal oxides, CNT and PPy, these heterostructures proficiently inhibited the restacking of Mxene nanosheets. Furthermore, the porous structure of Mxene supercapacitor has displayed substantial increase in performance, other practicable supercapacitors have also been designed apart from double symmetrical electrodes. Owing to their peculiar 2D layered

Table 4
Summary and comparison between MXenes and convectional 2D materials.

Material	Type of energy storage	Electrolyte solution	Capacity at different scan rates and their retention stability after specific cycles	References
Black phosphorus/graphene	LIB	1.0 M of $LiPF_6$ in EC/DEC/EMC at 1:1 ratio.	480 mAh/g at 100 mA/g, over 100 cycles	[128]
Graphene	LIB	1.0 M of $LiClO_4$ in EC/DEC	540 mAh/g	[129]
Phosphorene-graphene	NIB	1.0 M of $NaPF_6$ in EC/DEC along with 10% fluoroethylene carbonate	645 mAh/g at 10C and efficiency of 97.6 and 99.3%, after first 100 cycles.	[130]
Ti_2CT_x	NIB	1.0 M of $NaPF_6$ in EC/DEC	90 mAh/g and 40 mAh/g at 1 A/g and 5 A/g	[20]
$Ti_3C_2T_x$	NIB	1.0 M of H_2SO_4	900F/cm^3	[9]
$Ti_3C_2(OH)_{0.8}F_{1.2}$/Ag	LIB	1.0 M of $LiPF_6$ in EC/DEC/EMC	310 mAh/g at 1C after 800 cycles and 150 mAh/g at 50C after 5000cycles	[77]
Ti_3SiC_2	LIB	1.0 M of $LiPF_6$ in EC/DEC	After 140 cycles, 380 μAh/cm^2 (200 μA/cm^2)	[131]
Nb_2CT_x/CNT	LIB	1.0 M of $LiPF_6$ in EC/DEC	400 mAh/g at 0.5C	[83]
PVP-Sn(IV) @Ti_3C_2	LIB	1.0 M of $LiPF_6$ in EC/DEC	635 mAh/g at 100 mA/g, magnificent retention after 50 cycles	[81]
p-$Ti_3C_2T_x$/CNT	LIB	1.0 M of $LiPF_6$ in EC/DEC as 1:1 ratio	1250 mAh/g at 0.1C	[26]
$Ti_3C_2T_x$ hydrogel	Supercapacitor	Saturated solution K_2SO_4 or Ag/AgCl in 1 M KCl	1,500F/m^3 and areal capacitance up to 4F/cm^2	[22]

EC – ethylene carbonate, DEC- dimethyl carbonate and EMC -ethyl methyl carbonate.

architecture and efficient adsorption the gravimetric and volumetric capacitances of $Ti_3C_2T_x$ has been tested and determined by various practical methods, Table 4 has outlined brilliant performance of various MXene composites over present 2D materials in energy storage applications. It is noteworthy, that Ti_3C_2 only represents one example of family of MXenes, further evolvement and implication of these results shed light for developing high performance hybrid MXenes electrodes for energy storage devices, the potential of MXenes in energy harvesting applications is incredibly prodigious.

Declaration of Competing Interest

The authors declare that they have no known competing financial interests or personal relationships that could have appeared to influence the work reported in this paper.

Acknowledgements

The authors are thankful to Dr. C. P. Ramanarayanan, Vice-Chancellor of DIAT (DU), Pune for encouragement and support. The authors would like to thank Mr. Prakash Gore, Mr. Swaroop Gharde, and Mr. RaviPrakash Magisetty, for technical support provided during manuscript writing. The authors also acknowledge Mr. Rushikesh Ambekar, Mr. Deepak Prajapati, Mr. Kalpesh Kakulite, Mr. Jay Korde and Ms. Prasansha Rastogi for technical discussion and support. The authors are also thankful to the Editor and anonymous reviewers for improving the quality of the manuscript by their valuable comments and suggestions.

Appendix A. Supplementary data

Supplementary data to this article can be found online at https://doi.org/10.1016/j.cej.2019.123678.

References

[1] D.P. Dubal, N.R. Chodankar, D.-H. Kim, P. Gomez-Romero, Towards flexible solid-state supercapacitors for smart and wearable electronics, Chem. Soc. Rev. 47 (2018) 2065–2129, https://doi.org/10.1039/C7CS00505A.
[2] D. Er, J. Li, M. Naguib, Y. Gogotsi, V.B. Shenoy, Ti3C2 MXene as a high capacity electrode material for metal (Li, Na, K, Ca) ion batteries, ACS Appl. Mater. Interfaces (2014), https://doi.org/10.1021/am501144q.
[3] R. Yadav, A. Subhash, N. Chemmenchery, B. Kandasubramanian, Graphene and graphene oxide for fuel cell technology, Ind. Eng. Chem. Res. 57 (2018) 9333–9350, https://doi.org/10.1021/acs.iecr.8b02326.
[4] D. Xiong, X. Li, Z. Bai, S. Lu, Recent advances in layered Ti 3 C 2 T x MXene for electrochemical energy storage, Small 14 (2018) 1703419, https://doi.org/10.1002/smll.201703419.
[5] M.R. Lukatskaya, O. Mashtalir, C.E. Ren, Y. Dall'Agnese, P. Rozier, P.L. Taberna, M. Naguib, P. Simon, M.W. Barsoum, Y. Gogotsi, Cation Intercalation and High Volumetric Capacitance of Two-Dimensional Titanium Carbide, Science (80-.). 341 (2013) 1502–1505. https://doi.org/10.1126/science.1241488.
[6] M. Naguib, J. Come, B. Dyatkin, V. Presser, P.-L. Taberna, P. Simon, M.W. Barsoum, Y. Gogotsi, MXene: a promising transition metal carbide anode for lithium-ion batteries, Electrochem. Commun. 16 (2012) 61–64, https://doi.org/10.1016/j.elecom.2012.01.002.
[7] J. Luo, C. Wang, H. Wang, X. Hu, E. Matios, X. Lu, W. Zhang, X. Tao, W. Li, Pillared MXene with ultralarge interlayer spacing as a stable matrix for high performance sodium metal anodes, Adv. Funct. Mater. 29 (2019) 1805946, https://doi.org/10.1002/adfm.201805946.
[8] J. Yan, Y. Ma, C. Zhang, X. Li, W. Liu, X. Yao, S. Yao, S. Luo, polypyrrole–MXene coated textile-based flexible energy storage device, RSC Adv. 8 (2018) 39742–39748, https://doi.org/10.1039/C8RA08403C.
[9] B. Anasori, M.R. Lukatskaya, Y. Gogotsi, 2D metal carbides and nitrides (MXenes) for energy storage, Nat. Rev. Mater. 2 (2017) 16098, https://doi.org/10.1038/natrevmats.2016.98.
[10] Y. Sun, Q. Wu, G. Shi, Graphene based new energy materials, Energy Environ. Sci. 4 (2011) 1113, https://doi.org/10.1039/c0ee00683a.
[11] Q. Tang, Z. Zhou, P. Shen, Are MXenes Promising Anode Materials for Li Ion Batteries? Computational Studies on Electronic Properties and Li Storage Capability of Ti 3 C 2 and Ti 3 C 2 X 2 (X = F, OH) Monolayer, J. Am. Chem. Soc. 134 (2012) 16909–16916, https://doi.org/10.1021/ja308463r.
[12] Z. Ling, C.E. Ren, M.-Q. Zhao, J. Yang, J.M. Giammarco, J. Qiu, M.W. Barsoum, Y. Gogotsi, Flexible and conductive MXene films and nanocomposites with high capacitance, Proc. Natl. Acad. Sci. 111 (2014) 16676–16681, https://doi.org/10.1073/pnas.1414215111.
[13] O. Mashtalir, M. Naguib, V.N. Mochalin, Y. Dall'Agnese, M. Heon, M.W. Barsoum, Y. Gogotsi, Intercalation and delamination of layered carbides and carbonitrides, Nat. Commun. 4 (2013) 1716, https://doi.org/10.1038/ncomms2664.
[14] W. Zheng, P. Zhang, J. Chen, W.B. Tian, Y.M. Zhang, Z.M. Sun, In situ synthesis of CNTs@Ti 3 C 2 hybrid structures by microwave irradiation for high-performance anodes in lithium ion batteries, J. Mater. Chem. A 6 (2018) 3543–3551, https://doi.org/10.1039/c7ta10394h.
[15] J.-C. Lei, X. Zhang, Z. Zhou, Recent advances in MXene: Preparation, properties, and applications, Front. Phys. 10 (2015) 276–286, https://doi.org/10.1007/s11467-015-0493-x.
[16] M. Naguib, V.N. Mochalin, M.W. Barsoum, Y. Gogotsi, 25th Anniversary article: MXenes: a new family of two-dimensional materials, Adv. Mater. 26 (2014) 992–1005, https://doi.org/10.1002/adma.201304138.
[17] M. Naguib, R.R. Unocic, B.L. Armstrong, J. Nanda, Large-scale delamination of multi-layers transition metal carbides and carbonitrides "MXenes", Dalt. Trans. 44 (2015) 9353–9358, https://doi.org/10.1039/C5DT01247C.
[18] V.M. Hong Ng, H. Huang, K. Zhou, P.S. Lee, W. Que, J.Z. Xu, L.B. Kong, Recent progress in layered transition metal carbides and/or nitrides (MXenes) and their composites: synthesis and applications, J. Mater. Chem. A 5 (2017) 3039–3068, https://doi.org/10.1039/c6ta06772g.
[19] H. Zhang, X. Xin, H. Liu, H. Huang, N. Chen, Y. Xie, W. Deng, C. Guo, W. Yang, Enhancing lithium adsorption and diffusion toward extraordinary lithium storage capability of freestanding Ti 3 C 2 T x MXene, J. Phys. Chem. C 123 (2019) 2792–2800, https://doi.org/10.1021/acs.jpcc.8b11255.
[20] X. Wang, S. Kajiyama, H. Iinuma, E. Hosono, S. Oro, I. Moriguchi, M. Okubo, A. Yamada, Pseudocapacitance of MXene nanosheets for high-power sodium-ion hybrid capacitors, Nat. Commun. 6 (2015) 6544, https://doi.org/10.1038/ncomms7544.
[21] M. Ghidiu, M.R. Lukatskaya, M.-Q. Zhao, Y. Gogotsi, M.W. Barsoum, Conductive two-dimensional titanium carbide 'clay' with high volumetric capacitance, Nature (2014), https://doi.org/10.1038/nature13970.
[22] M.R. Lukatskaya, S. Kota, Z. Lin, M.-Q. Zhao, N. Shpigel, M.D. Levi, J. Halim, P.-L. Taberna, M.W. Barsoum, P. Simon, Y. Gogotsi, Ultra-high-rate pseudocapacitive energy storage in two-dimensional transition metal carbides, Nat. Energy 2 (2017) 17105, https://doi.org/10.1038/nenergy.2017.105.

[23] R. Cheng, T. Hu, H. Zhang, C. Wang, M. Hu, J. Yang, C. Cui, T. Guang, C. Li, C. Shi, P. Hou, X. Wang, Understanding the lithium storage mechanism of Ti 3 C 2 T x MXene, J. Phys. Chem. C 123 (2019) 1099–1109, https://doi.org/10.1021/acs.jpcc.8b10790.

[24] Y. Sun, D. Chen, Z. Liang, Two-dimensional MXenes for energy storage and conversion applications, Mater. Today Energy 5 (2017) 22–36, https://doi.org/10.1016/j.mtener.2017.04.008.

[25] Z.M. Sun, Progress in research and development on MAX phases: a family of layered ternary compounds, Int. Mater. Rev. 56 (2011) 143–166, https://doi.org/10.1179/1743280410Y.0000000001.

[26] C.E. Ren, M.-Q. Zhao, T. Makaryan, J. Halim, M. Boota, S. Kota, B. Anasori, M.W. Barsoum, Y. Gogotsi, Porous Two-dimensional transition metal carbide (MXene) flakes for high-performance Li-ion storage, ChemElectroChem 3 (2016) 689–693, https://doi.org/10.1002/celc.201600059.

[27] Y. Gogotsi, Transition metal carbides go 2D, Nat. Mater. 14 (2015) 1079–1080, https://doi.org/10.1038/nmat4386.

[28] M. Naguib, Y. Gogotsi, Synthesis of two-dimensional materials by selective extraction, Acc. Chem. Res. 48 (2015) 128–135, https://doi.org/10.1021/ar500346b.

[29] X. Chen, Y. Zhu, X. Zhu, W. Peng, Y. Li, G. Zhang, F. Zhang, X. Fan, Partially etched Ti 3 AlC 2 as a promising high-capacity lithium-ion battery anode, ChemSusChem 11 (2018) 2677–2680, https://doi.org/10.1002/cssc.201801200.

[30] M. Naguib, M. Kurtoglu, V. Presser, J. Lu, J. Niu, M. Heon, L. Hultman, Y. Gogotsi, M.W. Barsoum, Two-dimensional nanocrystals produced by exfoliation of Ti3AlC2, Adv. Mater. 23 (2011) 4248–4253, https://doi.org/10.1002/adma.201102306.

[31] S. Lai, J. Jeon, S.K. Jang, J. Xu, Y.J. Choi, J.H. Park, E. Hwang, S. Lee, Surface group modification and carrier transport properties of layered transition metal carbides (Ti 2 CT x, T: -OH, -F and -O), Nanoscale (2015), https://doi.org/10.1039/c5nr06513e.

[32] J. Zhou, X. Zha, F.Y. Chen, Q. Ye, P. Eklund, S. Du, Q. Huang, A Two-dimensional zirconium carbide by selective etching of Al 3 C 3 from nanolaminated Zr 3 Al 3 C 5, Angew. Chemie Int. Ed. 55 (2016) 5008–5013, https://doi.org/10.1002/anie.201510432.

[33] J. Halim, S. Kota, M.R. Lukatskaya, M. Naguib, M.-Q. Zhao, E.J. Moon, J. Pitock, J. Nanda, S.J. May, Y. Gogotsi, M.W. Barsoum, Synthesis and characterization of 2D molybdenum carbide (MXene), Adv. Funct. Mater. 26 (2016) 3118–3127, https://doi.org/10.1002/adfm.201505328.

[34] T.M. Gesing, W. Jeitschko, The crystal structures of Zr3Al3C5, ScAl3C3, and UAl3C3and their relation to the structures of U2Al3C4and Al4C3, J. Solid State Chem. 140 (1998) 396–401, https://doi.org/10.1006/jssc.1998.7907.

[35] X. Wang, C. Garnero, G. Rochard, D. Magne, S. Morisset, S. Hurand, P. Chartier, J. Rousseau, T. Cabioc'h, C. Coutanceau, V. Mauchamp, S. Célérier, A new etching environment (FeF 3/HCl) for the synthesis of two-dimensional titanium carbide MXenes: a route towards selective reactivity vs water, J. Mater. Chem. A 5 (2017) 22012–22023, https://doi.org/10.1039/C7TA01082F.

[36] C. Xu, L. Wang, Z. Liu, L. Chen, J. Guo, N. Kang, X.-L. Ma, H.-M. Cheng, W. Ren, Large-area high-quality 2D ultrathin Mo2C superconducting crystals, Nat. Mater. 14 (2015) 1135–1141, https://doi.org/10.1038/nmat4374.

[37] P. Urbankowski, B. Anasori, T. Makaryan, D. Er, S. Kota, P.L. Walsh, M. Zhao, V.B. Shenoy, M.W. Barsoum, Y. Gogotsi, Synthesis of two-dimensional titanium nitride Ti $_{4}$ $_{N}$ 3 (MXene), Nanoscale (2016), https://doi.org/10.1039/C6NR02253G.

[38] R. Fang, C. Lu, A. Chen, K. Wang, H. Huang, Y. Gan, C. Liang, J. Zhang, X. Tao, Y. Xia, W. Zhang, 2 D MXene-based energy storage materials: interfacial structure design and functionalization, ChemSusChem cssc.201902537 (2019), https://doi.org/10.1002/cssc.201902537.

[39] F. Liu, A. Zhou, J. Chen, H. Zhang, J. Cao, L. Wang, Q. Hu, Preparation and methane adsorption of two-dimensional carbide Ti2C, Adsorption 22 (2016) 915–922, https://doi.org/10.1007/s10450-016-9795-8.

[40] X. Wang, X. Shen, Y. Gao, Z. Wang, R. Yu, L. Chen, Atomic-scale recognition of surface structure and intercalation mechanism of Ti3C2X, J. Am. Chem. Soc. (2015), https://doi.org/10.1021/ja512820k.

[41] J. Halim, M.R. Lukatskaya, K.M. Cook, J. Lu, C.R. Smith, L.-Å. Näslund, S.J. May, L. Hultman, Y. Gogotsi, P. Eklund, M.W. Barsoum, Transparent conductive two-dimensional titanium carbide epitaxial thin films, Chem. Mater. 26 (2014) 2374–2381, https://doi.org/10.1021/cm500641a.

[42] J. Li, X. Yuan, C. Lin, Y. Yang, L. Xu, X. Du, J. Xie, J. Lin, J. Sun, Achieving high pseudocapacitance of 2D titanium carbide (MXene) by cation intercalation and surface modification, Adv. Energy Mater. 7 (2017) 1602725, https://doi.org/10.1002/aenm.201602725.

[43] K.D. Fredrickson, B. Anasori, Z.W. Seh, Y. Gogotsi, A. Vojvodic, Effects of applied potential and water intercalation on the surface chemistry of Ti 2 C and Mo 2 C MXenes, J. Phys. Chem. C 120 (2016) 28432–28440, https://doi.org/10.1021/acs.jpcc.6b09109.

[44] N.K. Chaudhari, H. Jin, B. Kim, D. San Baek, S.H. Joo, K. Lee, MXene: an emerging two-dimensional material for future energy conversion and storage applications, J. Mater. Chem. A 5 (2017) 24564–24579, https://doi.org/10.1039/C7TA09094C.

[45] X.F. Yu, J. Cheng, Z. Liu, Q. Li, W. Li, X. Yang, B. Xiao, Mg intercalation into Ti2C building block, Chem. Phys. Lett. (2015), https://doi.org/10.1016/j.cplett.2015.04.015.

[46] B. Anasori, Y. Xie, M. Beidaghi, J. Lu, B.C. Hosler, L. Hultman, P.R.C. Kent, Y. Gogotsi, M.W. Barsoum, Two-dimensional, ordered, double transition metals carbides (MXenes), ACS Nano 9 (2015) 9507–9516, https://doi.org/10.1021/acsnano.5b03591.

[47] C. Eames, M.S. Islam, Ion Intercalation into two-dimensional transition-metal carbides: global screening for new high-capacity battery materials, J. Am. Chem. Soc. 136 (2014) 16270–16276, https://doi.org/10.1021/ja508154e.

[48] M. Malaki, A. Maleki, R.S. Varma, MXenes and ultrasonication, J. Mater. Chem. A (2019), https://doi.org/10.1039/c9ta01850f.

[49] T. Hu, J. Wang, H. Zhang, Z. Li, M. Hu, X. Wang, Vibrational properties of Ti 3 C 2 and Ti 3 C 2 T 2 (T = O, F, OH) monosheets by first-principles calculations: a comparative study, Phys. Chem. Chem. Phys. 17 (2015) 9997–10003, https://doi.org/10.1039/C4CP05666C.

[50] J. Pang, R.G. Mendes, A. Bachmatiuk, L. Zhao, H.Q. Ta, T. Gemming, H. Liu, Z. Liu, M.H. Rummeli, Applications of 2D MXenes in energy conversion and storage systems, Chem. Soc. Rev. (2019), https://doi.org/10.1039/c8cs00324f.

[51] M. Khazaei, M. Arai, T. Sasaki, C.-Y. Chung, N.S. Venkataramanan, M. Estili, Y. Sakka, Y. Kawazoe, Novel electronic and magnetic properties of two-dimensional transition metal carbides and nitrides, Adv. Funct. Mater. 23 (2013) 2185–2192, https://doi.org/10.1002/adfm.201202502.

[52] H.-W. Wang, M. Naguib, K. Page, D.J. Wesolowski, Y. Gogotsi, Resolving the structure of Ti 3 C 2 T x MXenes through multilevel structural modeling of the atomic pair distribution function, Chem. Mater. 28 (2016) 349–359, https://doi.org/10.1021/acs.chemmater.5b04250.

[53] M.A. Hope, A.C. Forse, K.J. Griffith, M.R. Lukatskaya, M. Ghidiu, Y. Gogotsi, C.P. Grey, NMR reveals the surface functionalisation of Ti3C2 MXene, Phys. Chem. Chem. Phys. (2016), https://doi.org/10.1039/c6cp00330c.

[54] A.N. Enyashin, A.L. Ivanovskii, Structural and electronic properties and stability of MX enes Ti 2C and Ti3C2 functionalized by methoxy groups, J. Phys. Chem. C (2013), https://doi.org/10.1021/jp401820b.

[55] Y. Xie, M. Naguib, V.N. Mochalin, M.W. Barsoum, Y. Gogotsi, X. Yu, K.-W. Nam, X.-Q. Yang, A.I. Kolesnikov, P.R.C. Kent, Role of surface structure on Li-Ion energy storage capacity of two-dimensional transition-metal carbides, J. Am. Chem. Soc. 136 (2014) 6385–6394, https://doi.org/10.1021/ja501520b.

[56] J. Halim, K.M. Cook, M. Naguib, P. Eklund, Y. Gogotsi, J. Rosen, M.W. Barsoum, X-ray photoelectron spectroscopy of select multi-layered transition metal carbides (MXenes), Appl. Surf. Sci. 362 (2016) 406–417, https://doi.org/10.1016/j.apsusc.2015.11.089.

[57] M. Kurtoglu, M. Naguib, Y. Gogotsi, M.W. Barsoum, First principles study of two-dimensional early transition metal carbides, MRS Commun. (2012), https://doi.org/10.1557/mrc.2012.25.

[58] V.N. Borysiuk, V.N. Mochalin, Y. Gogotsi, Molecular dynamic study of the mechanical properties of two-dimensional titanium carbides Tin + 1Cn (MXenes), Nanotechnology (2015), https://doi.org/10.1088/0957-4484/26/26/265705.

[59] X.H. Zha, K. Luo, Q. Li, Q. Huang, J. He, X. Wen, S. Du, Role of the surface effect on the structural, electronic and mechanical properties of the carbide MXenes, EPL (2015), https://doi.org/10.1209/0295-5075/111/26007.

[60] A. Lipatov, H. Lu, M. Alhabeb, B. Anasori, A. Gruverman, Y. Gogotsi, A. Sinitskii, Elastic properties of 2D Ti 3 C 2 T x MXene monolayers and bilayers, Sci. Adv. 4 (2018), https://doi.org/10.1126/sciadv.aat0491.

[61] X. Wu, L. Hao, J. Zhang, X. Zhang, J. Wang, J. Liu, Polymer-Ti 3 C 2 T x composite membranes to overcome the trade-off in solvent resistant nanofiltration for alcohol-based system, J. Membr. Sci. (2016), https://doi.org/10.1016/j.memsci.2016.05.048.

[62] H. Zhang, L. Wang, Q. Chen, P. Li, A. Zhou, X. Cao, Q. Hu, Preparation, mechanical and anti-friction performance of MXene/polymer composites, Mater. Des. 92 (2016) 682–689, https://doi.org/10.1016/j.matdes.2015.12.084.

[63] K. Hantanasirisakul, M.-Q. Zhao, P. Urbankowski, J. Halim, B. Anasori, S. Kota, C.E. Ren, M.W. Barsoum, Y. Gogotsi, Fabrication of Ti 3 C 2 T x MXene transparent thin films with tunable optoelectronic properties, Adv. Electron. Mater. 2 (2016) 1600050, https://doi.org/10.1002/aelm.201600050.

[64] A. Ali, A. Belaidi, S. Ali, M.I. Helal, K.A. Mahmoud, Transparent and conductive Ti3C2Tx (MXene) thin film fabrication by electrohydrodynamic atomization technique, J. Mater. Sci. Mater. Electron. 27 (2016) 5440–5445, https://doi.org/10.1007/s10854-016-4447-z.

[65] C. Si, J. Zhou, Z. Sun, Half-metallic ferromagnetism and surface functionalization-induced metal-insulator transition in graphene-like two-dimensional Cr2C Crystals, ACS Appl. Mater. Interfaces (2015), https://doi.org/10.1021/acsami.5b05401.

[66] H. Kumar, N.C. Frey, L. Dong, B. Anasori, Y. Gogotsi, V.B. Shenoy, Tunable magnetism and transport properties in nitride MXenes, ACS Nano. (2017), https://doi.org/10.1021/acsnano.7b02578.

[67] Y. Xie, P.R.C. Kent, Hybrid density functional study of structural and electronic properties of functionalized Ti n + 1Xn (=C, N) monolayers, Phys. Rev. B 87 (2013) 235441, , https://doi.org/10.1103/PhysRevB.87.235441.

[68] D. Magne, V. Mauchamp, P. Chartier, T. Cabioc, Site-projected electronic structure of two-dimensional Ti 3 C 2 MXene: the role of the surface functionalization groups †, Phys. Chem. Chem. Phys. (2016) 14–16, https://doi.org/10.1039/c6cp05985f.

[69] H. Kim, Z. Wang, H.N. Alshareef, MXetronics: electronic and photonic applications of MXenes, Nano Energy. 60 (2019) 179–197, https://doi.org/10.1016/j.nanoen.2019.03.020.

[70] Y. Zhang, X.-H. Zha, K. Luo, N. Qiu, Y. Zhou, J. He, Z. Chai, Z. Huang, Q. Huang, Y. Liang, S. Du, Tuning the electrical conductivity of Ti 2 CO 2 MXene by varying the layer thickness and applying strains, J. Phys. Chem. C 123 (2019) 6802–6811, https://doi.org/10.1021/acs.jpcc.8b10888.

[71] X. Li, C. Wang, Y. Cao, G. Wang, Functional MXene materials: progress of their applications, Chem. – An Asian J. 13 (2018) 2742–2757, https://doi.org/10.1002/asia.201800543.

[72] M.-Q. Zhao, M. Torelli, C.E. Ren, M. Ghidiu, Z. Ling, B. Anasori, M.W. Barsoum, Y. Gogotsi, 2D titanium carbide and transition metal oxides hybrid electrodes for

Li-ion storage, Nano Energy 30 (2016) 603–613, https://doi.org/10.1016/j.nanoen.2016.10.062.
[73] M.D. Levi, M.R. Lukatskaya, S. Sigalov, M. Beidaghi, N. Shpigel, L. Daikhin, D. Aurbach, M.W. Barsoum, Y. Gogotsi, Solving the capacitive paradox of 2D MXene using electrochemical quartz-crystal admittance and in situ electronic conductance measurements, Adv. Energy Mater. 5 (2015) 1400815, https://doi.org/10.1002/aenm.201400815.
[74] C.J. Zhang, B. Anasori, A. Seral-Ascaso, S.-H. Park, N. McEvoy, A. Shmeliov, G.S. Duesberg, J.N. Coleman, Y. Gogotsi, V. Nicolosi, Transparent, flexible, and conductive 2D titanium carbide (MXene) films with high volumetric capacitance, Adv. Mater. 29 (2017) 1702678, https://doi.org/10.1002/adma.201702678.
[75] S.J. Kim, M. Naguib, M. Zhao, C. Zhang, H.-T. Jung, M.W. Barsoum, Y. Gogotsi, High mass loading, binder-free MXene anodes for high areal capacity Li-ion batteries, Electrochim. Acta 163 (2015) 246–251, https://doi.org/10.1016/j.electacta.2015.02.132.
[76] Q. Fu, J. Wen, N. Zhang, L. Wu, M. Zhang, S. Lin, H. Gao, X. Zhang, Free-standing Ti 3 C 2 T x electrode with ultrahigh volumetric capacitance, RSC Adv. 7 (2017) 11998–12005, https://doi.org/10.1039/C7RA00126F.
[77] G. Zou, Z. Zhang, J. Guo, B. Liu, Q. Zhang, C. Fernandez, Q. Peng, Synthesis of MXene/Ag composites for extraordinary long cycle lifetime lithium storage at high rates, ACS Appl. Mater. Interfaces 8 (2016) 22280–22286, https://doi.org/10.1021/acsami.6b08089.
[78] M. Naguib, J. Halim, J. Lu, K.M. Cook, L. Hultman, Y. Gogotsi, M.W. Barsoum, New two-dimensional niobium and vanadium carbides as promising materials for li-ion batteries, J. Am. Chem. Soc. (2013), https://doi.org/10.1021/ja405735d.
[79] Z. Lin, D. Sun, Q. Huang, J. Yang, M.W. Barsoum, X. Yan, Carbon nanofiber bridged two-dimensional titanium carbide as a superior anode for lithium-ion batteries, J. Mater. Chem. A (2015), https://doi.org/10.1039/c5ta01855b.
[80] M. Boota, B. Anasori, C. Voigt, M.Q. Zhao, M.W. Barsoum, Y. Gogotsi, Pseudocapacitive electrodes produced by oxidant-free polymerization of pyrrole between the layers of 2D titanium carbide (MXene), Adv. Mater. (2016), https://doi.org/10.1002/adma.201504705.
[81] J. Luo, X. Tao, J. Zhang, Y. Xia, H. Huang, L. Zhang, Y. Gan, C. Liang, W. Zhang, Sn 4+ ion decorated highly conductive Ti 3 C 2 MXene: promising lithium-ion anodes with enhanced volumetric capacity and cyclic performance, ACS Nano 10 (2016) 2491–2499, https://doi.org/10.1021/acsnano.5b07333.
[82] Y. Dall'Agnese, P. Rozier, P.-L. Taberna, Y. Gogotsi, P. Simon, Capacitance of two-dimensional titanium carbide (MXene) and MXene/carbon nanotube composites in organic electrolytes, J. Power Sources. 306 (2016) 510–515, https://doi.org/10.1016/j.jpowsour.2015.12.036.
[83] O. Mashtalir, M.R. Lukatskaya, M.-Q. Zhao, M.W. Barsoum, Y. Gogotsi, Amine-assisted delamination of Nb 2 C MXene for li-ion energy storage devices, Adv. Mater. 27 (2015) 3501–3506, https://doi.org/10.1002/adma.201500604.
[84] A. Byeon, A.M. Glushenkov, B. Anasori, P. Urbankowski, J. Li, B.W. Byles, B. Blake, K.L. Van Aken, S. Kota, E. Pomerantseva, J.W. Lee, Y. Chen, Y. Gogotsi, Lithium-ion capacitors with 2D Nb 2 CT x (MXene) – carbon nanotube electrodes, J. Power Sour. 326 (2016) 686–694, https://doi.org/10.1016/j.jpowsour.2016.03.066.
[85] B.-M. Jun, S. Kim, J. Heo, C.M. Park, N. Her, M. Jang, Y. Huang, J. Han, Y. Yoon, Review of MXenes as new nanomaterials for energy storage/delivery and selected environmental applications, Nano Res. 12 (2019) 471–487, https://doi.org/10.1007/s12274-018-2225-3.
[86] M. Hu, Z. Li, H. Zhang, T. Hu, C. Zhang, Z. Wu, X. Wang, Self-assembled Ti 3 C 2 T x MXene film with high gravimetric capacitance, Chem. Commun. 51 (2015) 13531–13533, https://doi.org/10.1039/C5CC04722F.
[87] Q.X. Xia, N.M. Shinde, J.M. Yun, T. Zhang, R.S. Mane, S. Mathur, K.H. Kim, Bismuth oxychloride/MXene symmetric supercapacitor with high volumetric energy density, Electrochim. Acta 271 (2018) 351–360, https://doi.org/10.1016/j.electacta.2018.03.168.
[88] X. Zhang, Y. Liu, S. Dong, J. Yang, X. Liu, Self-assembled three-dimensional Ti3C2Tx nanosheets network on carbon cloth as flexible electrode for supercapacitors, Appl. Surf. Sci. 485 (2019) 1–7, https://doi.org/10.1016/j.apsusc.2019.04.197.
[89] J. Luo, W. Zhang, H. Yuan, C. Jin, L. Zhang, H. Huang, C. Liang, Y. Xia, J. Zhang, Y. Gan, X. Tao, Pillared structure design of MXene with ultralarge interlayer spacing for high-performance lithium-ion capacitors, ACS Nano 11 (2017) 2459–2469, https://doi.org/10.1021/acsnano.6b07668.
[90] J. Luo, C. Fang, C. Jin, H. Yuan, O. Sheng, R. Fang, W. Zhang, H. Huang, Y. Gan, Y. Xia, C. Liang, J. Zhang, W. Li, X. Tao, Tunable pseudocapacitance storage of MXene by cation pillaring for high performance sodium-ion capacitors, J. Mater. Chem. A 6 (2018) 7794–7806, https://doi.org/10.1039/C8TA02068J.
[91] Y. Xie, Y. Dall'Agnese, M. Naguib, Y. Gogotsi, M.W. Barsoum, H.L. Zhuang, P.R.C. Kent, Prediction and characterization of MXene nanosheet anodes for non-lithium-ion Batteries, ACS Nano. 8 (2014) 9606–9615, https://doi.org/10.1021/nn503921j.
[92] S. Guo, J. Yi, Y. Sun, H. Zhou, Recent advances in titanium-based electrode materials for stationary sodium-ion batteries, Energy Environ. Sci. 9 (2016) 2978–3006, https://doi.org/10.1039/C6EE01807F.
[93] M.Q. Zhao, X. Xie, C.E. Ren, T. Makaryan, B. Anasori, G. Wang, Y. Gogotsi, Hollow MXene spheres and 3D macroporous MXene frameworks for na-ion storage, Adv. Mater. (2017), https://doi.org/10.1002/adma.201702410.
[94] J. Luo, J. Zheng, J. Nai, C. Jin, H. Yuan, O. Sheng, Y. Liu, R. Fang, W. Zhang, H. Huang, Y. Gan, Y. Xia, C. Liang, J. Zhang, W. Li, X. Tao, Atomic sulfur covalently engineered interlayers of Ti 3 C 2 MXene for ultra-fast sodium-ion storage by enhanced pseudocapacitance, Adv. Funct. Mater. 29 (2019) 1808107, https://doi.org/10.1002/adfm.201808107.
[95] M. Naguib, R.A. Adams, Y. Zhao, D. Zemlyanov, A. Varma, J. Nanda, V.G. Pol, Electrochemical performance of MXenes as K-ion battery anodes, Chem. Commun. 53 (2017) 6883–6886, https://doi.org/10.1039/C7CC02026K.
[96] P. Li, J. Zhu, A.D. Handoko, R. Zhang, H. Wang, D. Legut, X. Wen, Z. Fu, Z.W. Seh, Q. Zhang, High-throughput theoretical optimization of the hydrogen evolution reaction on MXenes by transition metal modification, J. Mater. Chem. A 6 (2018) 4271–4278, https://doi.org/10.1039/C8TA00173A.
[97] J. Di, C. Yan, A.D. Handoko, Z.W. Seh, H. Li, Z. Liu, Ultrathin two-dimensional materials for photo- and electrocatalytic hydrogen evolution, Mater. Today 21 (2018) 749–770, https://doi.org/10.1016/j.mattod.2018.01.034.
[98] Z.W. Seh, K.D. Fredrickson, B. Anasori, J. Kibsgaard, A.L. Strickler, M.R. Lukatskaya, Y. Gogotsi, T.F. Jaramillo, A. Vojvodic, Two-dimensional molybdenum carbide (MXene) as an efficient electrocatalyst for hydrogen evolution, ACS Energy Lett. (2016), https://doi.org/10.1021/acsenergylett.6b00247.
[99] A.D. Handoko, K.D. Fredrickson, B. Anasori, K.W. Convey, L.R. Johnson, Y. Gogotsi, A. Vojvodic, Z.W. Seh, Tuning the basal plane functionalization of two-dimensional metal carbides (MXenes) to control hydrogen evolution activity, ACS Appl. Energy Mater. 1 (2018) 173–180, https://doi.org/10.1021/acsaem.7b00054.
[100] A.D. Handoko, K.H. Khoo, T.L. Tan, H. Jin, Z.W. Seh, Establishing new scaling relations on two-dimensional MXenes for CO 2 electroreduction, J. Mater. Chem. A 6 (2018) 21885–21890, https://doi.org/10.1039/C8TA06567E.
[101] A.D. Handoko, F. Wei, B.S. Jenndy, Z.W. Seh Yeo, Understanding heterogeneous electrocatalytic carbon dioxide reduction through operando techniques, Nat. Catal. 1 (2018) 922–934, https://doi.org/10.1038/s41929-018-0182-6.
[102] A.D. Handoko, S.N. Steinmann, Z.W. Seh, Theory-guided materials design: two-dimensional MXenes in electro- and photocatalysis, Nanoscale Horizons 4 (2019) 809–827, https://doi.org/10.1039/C9NH00100J.
[103] F. Shahzad, M. Alhabeb, C.B. Hatter, B. Anasori, S.M. Hong, C.M. Koo, Y. Gogotsi, Electromagnetic interference shielding with 2D transition metal carbides (MXenes), Science 80 (2016), https://doi.org/10.1126/science.aag2421.
[104] A. Joshi, A. Bajaj, R. Singh, P.S. Alegaonkar, K. Balasubramanian, S. Datar, Graphene nanoribbon–PVA composite as EMI shielding material in the X band, Nanotechnology 24 (2013) 455705, , https://doi.org/10.1088/0957-4484/24/45/455705.
[105] J. Diao, M. Hu, Z. Lian, Z. Li, H. Zhang, F. Huang, B. Li, X. Wang, D.S. Su, H. Liu, Ti 3 C 2 T x MXene catalyzed ethylbenzene dehydrogenation: active sites and mechanism exploration from both experimental and theoretical aspects, ACS Catal. 8 (2018) 10051–10057, https://doi.org/10.1021/acscatal.8b02002.
[106] D. Zhao, Z. Chen, W. Yang, S. Liu, X. Zhang, Y. Yu, W.-C. Cheong, L. Zheng, F. Ren, G. Ying, X. Cao, D. Wang, Q. Peng, G. Wang, C. Chen, MXene (Ti 3 C 2) vacancy-confined single-atom catalyst for efficient functionalization of CO 2, J. Am. Chem. Soc. 141 (2019) 4086–4093, https://doi.org/10.1021/jacs.8b13579.
[107] H. Zhang, Z. Wang, Q. Zhang, F. Wang, Y. Liu, Ti3C2 MXenes nanosheets catalyzed highly efficient electrogenerated chemiluminescence biosensor for the detection of exosomes, Biosens. Bioelectron. 124–125 (2019) 184–190, https://doi.org/10.1016/j.bios.2018.10.016.
[108] M. Soleymaniha, M.-A. Shahbazi, A.R. Rafieerad, A. Maleki, A. Amiri, Promoting role of MXene nanosheets in biomedical sciences: therapeutic and biosensing innovations, Adv. Healthc. Mater. 8 (2019) 1801137, https://doi.org/10.1002/adhm.201801137.
[109] X. Peng, Y. Zhang, D. Lu, Y. Guo, S. Guo, Ultrathin Ti3C2 nanosheets based "off-on" fluorescent nanoprobe for rapid and sensitive detection of HPV infection, Sensors Actuat. B Chem. 286 (2019) 222–229, https://doi.org/10.1016/j.snb.2019.01.158.
[110] A. Szuplewska, D. Kulpińska, A. Dybko, A.M. Jastrzębska, T. Wojciechowski, A. Rozmysłowska, M. Chudy, I. Grabowska-Jadach, W. Ziemkowska, Z. Brzózka, A. Olszyna, 2D Ti2C (MXene) as a novel highly efficient and selective agent for photothermal therapy, Mater. Sci. Eng. C 98 (2019) 874–886, https://doi.org/10.1016/j.msec.2019.01.021.
[111] H.-J. Koh, S.J. Kim, K. Maleski, S.-Y. Cho, Y.-J. Kim, C.W. Ahn, Y. Gogotsi, H.-T. Jung, Enhanced selectivity of MXene gas sensors through metal ion intercalation in situ X-ray diffraction study, ACS Sens. 4 (2019) 1365–1372, https://doi.org/10.1021/acssensors.9b00310.
[112] A.M. Jastrzębska, E. Karwowska, T. Wojciechowski, W. Ziemkowska, A. Rozmysłowska, L. Chlubny, A. Olszyna, The atomic structure of Ti2C and Ti3C2 MXenes is responsible for their antibacterial activity toward E. coli bacteria, J. Mater. Eng. Perform. 28 (2019) 1272–1277, https://doi.org/10.1007/s11665-018-3223-z.
[113] A. Shahzad, M. Nawaz, M. Moztahida, J. Jang, K. Tahir, J. Kim, Y. Lim, V.S. Vassiliadis, S.H. Woo, D.S. Lee, Ti3C2Tx MXene core-shell spheres for ultrahigh removal of mercuric ions, Chem. Eng. J. 368 (2019) 400–408, https://doi.org/10.1016/j.cej.2019.02.160.
[114] W. Zhi, S. Xiang, R. Bian, R. Lin, K. Wu, T. Wang, D. Cai, Study of MXene-filled polyurethane nanocomposites prepared via an emulsion method, Compos. Sci. Technol. 168 (2018) 404–411, https://doi.org/10.1016/j.compscitech.2018.10.026.
[115] G. Ding, K. Zeng, K. Zhou, Z. Li, Y. Zhou, Y. Zhai, L. Zhou, X. Chen, S.-T. Han, Configurable multi-state non-volatile memory behaviors in Ti 3 C 2 nanosheets, Nanoscale 11 (2019) 7102–7110, https://doi.org/10.1039/C9NR00747D.
[116] Z. Zhou, J. Liu, X. Zhang, D. Tian, Z. Zhan, C. Lu, Ultrathin MXene/calcium alginate aerogel film for high-performance electromagnetic interference shielding, Adv. Mater. Interfaces 6 (2019) 1802040, https://doi.org/10.1002/admi.201802040.
[117] K. Rasool, M. Helal, A. Ali, C.E. Ren, Y. Gogotsi, K.A. Mahmoud, Antibacterial activity of Ti 3 C 2 T x MXene, ACS Nano 10 (2016) 3674–3684, https://doi.org/

10.1021/acsnano.6b00181.
[118] J. Zhu, E. Ha, G. Zhao, Y. Zhou, D. Huang, G. Yue, L. Hu, N. Sun, Y. Wang, L.Y.S. Lee, C. Xu, K.-Y. Wong, D. Astruc, P. Zhao, Recent advance in MXenes: A promising 2D material for catalysis, sensor and chemical adsorption, Coord. Chem. Rev. 352 (2017) 306–327, https://doi.org/10.1016/j.ccr.2017.09.012.
[119] Y. Gao, L. Wang, Z. Li, A. Zhou, Q. Hu, X. Cao, Preparation of MXene-Cu2O nanocomposite and effect on thermal decomposition of ammonium perchlorate, Solid State Sci. 35 (2014) 62–65, https://doi.org/10.1016/j.solidstatesciences.2014.06.014.
[120] S. Kumar, Y. Lei, N.H. Alshareef, M.A. Quevedo-Lopez, K.N. Salama, Biofunctionalized two-dimensional Ti3C2 MXenes for ultrasensitive detection of cancer biomarker, Biosens. Bioelectron. 121 (2018) 243–249, https://doi.org/10.1016/j.bios.2018.08.076.
[121] L. Wang, W. Tao, L. Yuan, Z. Liu, Q. Huang, Z. Chai, J.K. Gibson, W. Shi, Rational control of the interlayer space inside two-dimensional titanium carbides for highly efficient uranium removal and imprisonment, Chem. Commun. 53 (2017) 12084–12087, https://doi.org/10.1039/C7CC06740B.
[122] S.J. Kim, H.-J. Koh, C.E. Ren, O. Kwon, K. Maleski, S.-Y. Cho, B. Anasori, C.-K. Kim, Y.-K. Choi, J. Kim, Y. Gogotsi, H.-T. Jung, Metallic Ti 3 C 2 T x MXene gas sensors with ultrahigh signal-to-noise ratio, ACS Nano 12 (2018) 986–993, https://doi.org/10.1021/acsnano.7b07460.
[123] R. Malik, Maxing out water desalination with MXenes, Joule 2 (2018) 591–593, https://doi.org/10.1016/j.joule.2018.04.001.
[124] X. Han, J. Huang, H. Lin, Z. Wang, P. Li, Y. Chen, 2D Ultrathin MXene-based drug-delivery nanoplatform for synergistic photothermal ablation and chemotherapy of cancer, Adv. Healthc. Mater. (2018), https://doi.org/10.1002/adhm.201701394.
[125] H. Lin, X. Wang, L. Yu, Y. Chen, J. Shi, Two-dimensional ultrathin MXene ceramic nanosheets for photothermal conversion, Nano Lett. 17 (2017) 384–391, https://doi.org/10.1021/acs.nanolett.6b04339.
[126] Z. Wei, Z. Peigen, T. Wubian, Q. Xia, Z. Yamei, S. ZhengMing, Alkali treated Ti3C2Tx MXenes and their dye adsorption performance, Mater. Chem. Phys. (2018), https://doi.org/10.1016/j.matchemphys.2017.12.034.
[127] Q. Zhang, J. Teng, G. Zou, Q. Peng, Q. Du, T. Jiao, J. Xiang, Efficient phosphate sequestration for water purification by unique sandwich-like MXene/magnetic iron oxide nanocomposites, Nanoscale 8 (2016) 7085–7093, https://doi.org/10.1039/C5NR09303A.
[128] A.E. Del Rio Castillo, V. Pellegrini, H. Sun, J. Buha, D.A. Dinh, E. Lago, A. Ansaldo, A. Capasso, L. Manna, F. Bonaccorso, Exfoliation of few-layer black phosphorus in low-boiling-point solvents and its application in li-ion batteries, Chem. Mater. (2018), https://doi.org/10.1021/acs.chemmater.7b04628.
[129] E.J. Yoo, J. Kim, E. Hosono, H.S. Zhou, T. Kudo, I. Honma, Large reversible Li storage of graphene nanosheet families for use in rechargeable lithium ion batteries, Nano Lett. (2008), https://doi.org/10.1021/nl800957b.
[130] J. Sun, H.-W. Lee, M. Pasta, H. Yuan, G. Zheng, Y. Sun, Y. Li, Y. Cui, A phosphorene–graphene hybrid material as a high-capacity anode for sodium-ion batteries, Nat. Nanotechnol. 10 (2015) 980–985, https://doi.org/10.1038/nnano.2015.194.
[131] A.T. Tesfaye, O. Mashtalir, M. Naguib, M.W. Barsoum, Y. Gogotsi, T. Djenizian, Anodized Ti3SiC2 As an anode material for li-ion microbatteries, ACS Appl. Mater. Interfaces (2016), https://doi.org/10.1021/acsami.6b03528.